UNIVERSIDADE DO VALE DO RIO DOS SINOS - UNISINOS
UNIDADE ACADÊMICA DE PESQUISA E PÓS-GRADUAÇÃO
PROGRAMA DE PÓS-GRADUAÇÃO EM GEOLOGIA
NÍVEL MESTRADO

MÁRCIO CARDOSO JÚNIOR

EVOLUÇÃO TERMAL DE POTENCIAIS RESERVATÓRIOS NA PORÇÃO LESTE DA BACIA DO PARNAÍBA

SÃO LEOPOLDO
2018

Márcio Cardoso Júnior

EVOLUÇÃO TERMAL DE POTENCIAIS RESERVATÓRIOS NA PORÇÃO LESTE DA BACIA DO PARNAÍBA

Artigo apresentado como requisito parcial para obtenção do título de Mestre em Geologia, pelo Programa de Pós-Graduação em Geologia da Universidade do Vale do Rio dos Sinos - UNISINOS

Orientador: Prof. Dr. Farid Chemale Júnior

Coorientadora: Dra. Christie Helouise Engelmann de Oliveira

São Leopoldo

2018

C268e Cardoso Júnior, Márcio.

Evolução termal de potenciais reservatórios na porção leste da bacia do Parnaíba / Márcio Cardoso Júnior. – 2018.

68 f. : il. ; 30 cm.

Dissertação (mestrado) – Universidade do Vale do Rio dos Sinos, Programa de Pós-Graduação em Geologia, 2018.

"Orientador: Prof. Dr. Farid Chemale Júnior; coorientadora: Dra. Christie Helouise Engelmann de Oliveira."

1. Formação Poti. 2. Termocronologia por traço de fissão. 3. Reservatórios de gás. I. Título.

CDU 55

Dados Internacionais de Catalogação na Publicação (CIP)
(Bibliotecário: Flávio Nunes – CRB 10/1298)

AGRADECIMENTOS

Gostaria de agradecer a todos que durante o período do meu mestrado contribuíram para a realização desta dissertação, e especialmente:

- Ao Projeto POTI ANP-UnB-PGN pelos custos de viagem de campo e pelas amostras utilizadas neste trabalho;

- A CAPES pela bolsa PROSUC de estudo;

- Ao meu orientador Farid Chemale Jr. pela confiança e a oportunidade de desenvolver este trabalho, e pelo auxílio durante todo o mestrado;

- A minha coorientadora Christie H. E. de Oliveira pelas empolgantes discussões e pelos muitos momentos de trabalho compartilhado, além de sua grande amizade;

- Aos meus pais, Márcio Cardoso e Ana Beatriz Amboni que sempre me deram muito suporte e estão presentes ao meu lado para me auxiliar em minhas decisões;

- A minha colega e amiga Ariane S. da Silveira, quem me incentivou a entrar no mestrado e sempre me passa valiosos conselhos;

- Aos professores do PPG em Geologia que me passaram seus conhecimentos e vasta experiência, além de me ajudarem na construção desta dissertação;

- E aos meus colegas de mestrado e amigos com quem tive momentos de descontração e boas conversas, entre eles, Franciele Trentin, Laís Vieira, Mauro Daniel R. Bruno, Lucas R. Norenberg, Cândido Hanauer, Marcelo K. de Souza, Henrique A. Lopes, Ricardo Paiva e Valessa Araújo.

RESUMO

Nas últimas décadas, a Bacia do Parnaíba vem sendo assunto de estudo desde que foi descoberto seu alto potencial para exploração de gás natural. Neste escopo, a área de estudo deste trabalho está localizada na porção leste da bacia, região nordeste do Brasil, na qual afloram arenitos e siltitos das formações Cabeças (Devoniano) e Poti (Carbonífero), rochas reservatório da Bacia do Parnaíba. Subordinadamente, rochas magmáticas estão presentes correspondentes a dois eventos intrusivos de idade Mesozóica atribuídas às formações Mosquito e Sardinha. O primeiro evento é relacionado à ruptura entre a América do Norte e a América do Sul, e o segundo, entre a América do Sul e a África, cujos processos de intrusão magmática nas rochas sedimentares paleozóicas alteraram não somente as características petrográficas destas rochas, mas também modificaram as propriedades das rochas reservatório na bacia, sendo essas alterações identificadas durante etapas exploratórias. Foram coletadas amostras de rochas sedimentares em furos de sondagem e afloramentos, nas quais foram aplicados métodos de Termocronologia por Traços de Fissão em apatita e zircão, e petrografia, com o objetivo de integrar os dados de história térmica com as propriedades físicas das rochas, relacionando aos sistemas petrolíferos da região. Os resultados de Traços de Fissão em apatita e zircão indicam que o evento magmático da Formação Sardinha (Cretáceo) foi o de maior influência nesta porção da bacia. Em porções próximas as rochas magmáticas, as paleotemperaturas superaram 300 °C, condição que alterou os reservatórios. As altas temperaturas mobilizaram fluidos hidrotermais que alteraram as rochas pela dissolução de minerais e precipitação de cimento carbonático nos espaços porosos. Em porções onde a influência térmica foi atenuada, em termos de paleotemperatura máxima, as condições se tornam favoráveis para a não alteração térmica dos reservatórios.

Palavras-Chave: Formação Poti, Termocronologia por Traço de Fissão, Reservatório de Gás.

ABSTRACT

In the last few decades, the Parnaíba Basin is being subject of study since it was discovered its high potential on natural gas exploration. In this scope, the study area is located on the eastern part of the basin, northern region of Brazil, in which outcrop sandstones and siltstones of the Cabeças (Devonian) and Poti (Carboniferous) Formation, reservoir rocks of Parnaíba Basin. Subordinately, magmatic rocks are present corresponding to two intrusive events of Mesozoic ages attributed to the Mosquito and Sardinha formations. The first event is related to the breakup between the North America and South America, and the second, between South America and Africa, whose processes of magmatic intrusion in the Paleozoic rocks changed not only the petrographic characteristics of these rocks, but also modified the properties of the reservoir rocks in the basin, being these alterations identified during exploration stages. It was collected samples of sedimentary rocks in drilled core and outcrops, in which were applied method of Thermochronology by Fission-tracks in apatite and zircon, and petrography, with the objective to integrate data of thermal history and physical properties of the rocks, relating to petroleum systems in the region. The results of Fission-tracks in apatite and zircon indicated that the magmatic event of the Sardinha Formation (Cretaceous) was the major influence in the portion of the basin. In near portion of the magmatic rocks, the paleotemperatures have overcome 300 °C, condition that altered the reservoirs. The high temperatures mobilized hydrothermal fluids which altered the rocks by dissolving minerals and precipitation of carbonate cement in the pore space. In portions where the thermal influence is attenuated, in terms of maximum paleotemperature, the conditions become favorable for the non-thermal alteration of reservoirs.

Keywords: Poti Formation, Thermochronology by Fission-tracks, Gas Reservoir.

LISTA DE FIGURAS

LISTA DE FIGURAS DO ARTIGO

LISTA DE TABELAS

SUMÁRIO

APRESENTAÇÃO

A Bacia do Parnaíba apresenta um alto potencial exploratório para reservatórios de gás nas formações Poti e Cabeças. A qualidade destes reservatórios é dependente da presença dos dois pulsos intrusivos ocorridos durante o período Mesozóico. Especificamente, o aquecimento provocado pelas rochas ígneas modificou os parâmetros físicos e a maturação dos hidrocarbonetos das rochas sedimentares adjacentes, tanto nas rochas geradoras, como nas rochas reservatório. Os processos de aquecimento ligados aos pulsos magmáticos podem ter influência direta no comportamento heterogêneo no que tange ao processo de extração de gás.

Sendo assim, o principal objetivo desta dissertação é determinar os efeitos na qualidade dos níveis reservatório potenciais das formações Poti e Cabeças pela influência térmica das rochas intrusivas. Os objetivos secundários são: determinar a variação de temperatura próxima às rochas intrusivas e as propriedades diagenéticas das rochas sedimentares potenciais para reservatórios de gás. A determinação dos efeitos térmicos nas rochas reservatório foi realizada por meio de estudos petrográficos em lâminas delgadas e análises termocronológicas por traços de fissão em apatita e zircão.

Esta dissertação faz parte do projeto de pesquisa e desenvolvimento executado pelo Instituto de Geociências da Universidade de Brasília (UnB) com participação da Fundação de Empreendimentos Científicos e Tecnológicos (FINATEC) Parnaíba Gás Natural (PGN), Agência Nacional do Petróleo, Gás e Biocombustíveis (ANP), denominado de POTI ANP-UnB-PGN e coordenado pelos professores Carlos Emanoel de Souza Cruz e Carlos Jorge de Abreu. Durante a realização do projeto foi realizada uma saída de campo (16/04/2017 – 21/04/2017) para coleta de 10 amostras (testemunho e afloramento) próximas aos corpos magmáticos, a fim de aplicar os métodos enunciados acima. Os resultados obtidos culminaram na produção do manuscrito “THERMAL HISTORY OF POTENTIAL GAS RESERVOIR

ROCKS IN THE EASTERN PARNAÍBA BASIN, BRAZIL", posicionado ao fim deste volume, no qual são elencadas discussões e conclusões.

A BACIA DO PARNAÍBA E OS SISTEMAS PETROLÍFEROS

A Bacia do Parnaíba cobre uma área aproximada de 600.000 Km², com seu maior diâmetro na direção nordeste/sudoeste, recobrindo parte dos estados do Piauí, Maranhão, Pará, Tocantins, Ceará e Bahia (Fig. 1). A bacia está posicionada sobre um embasamento constituído de rochas sedimentares, ígneas e metamórficas, datadas do Arqueano ao Ordoviciano (VAZ et al., 2007). Almeida e Carneiro (2004) indicam que a subsidência inicial da bacia estaria ligada a eventos térmicos tardi- ou pós-orogênicos do Ciclo Brasiliano, citados pelos autores como "Estádio de Transição", no qual começaram a se desenvolver registros sedimentares em zonas deprimidas por falhamentos indicados por Oliveira e Mohriak (2003) em uma fase *rift*, pré-sinéclise.

O registro sedimentar da fase sinéclise da Bacia do Parnaíba é dividido em cinco supersequências: Siluriana, Mesodevoniana-Eocarbonífera, Neocarbonífera-Eotriássica, Jurássica e Cretácea, correspondendo a ciclos transgressivos-regressivos. A bacia tem uma espessura máxima de 3.500 metros no depocentro principal, o que indica uma lenta subsidência devido à pequena espessura de sedimentos e amplo intervalo de tempo (VAZ et al., 2007).

A Supersequência Siluriana é formada pelo Grupo Serra Grande, correspondendo a um ciclo transgressivo-regressivo completo depositado sobre o embasamento de idade proterozóica a cambriana. O grupo é constituído pelas formações Ipú, Tianguá e Jaicós. As rochas estão presentes em toda a extensão da bacia, aflorando na borda leste sobre o embasamento. O contato entre as formações é concordante, e a Formação Tianguá inclui a superfície de inundação máxima do Grupo Serra Grande (VAZ et al., 2007).

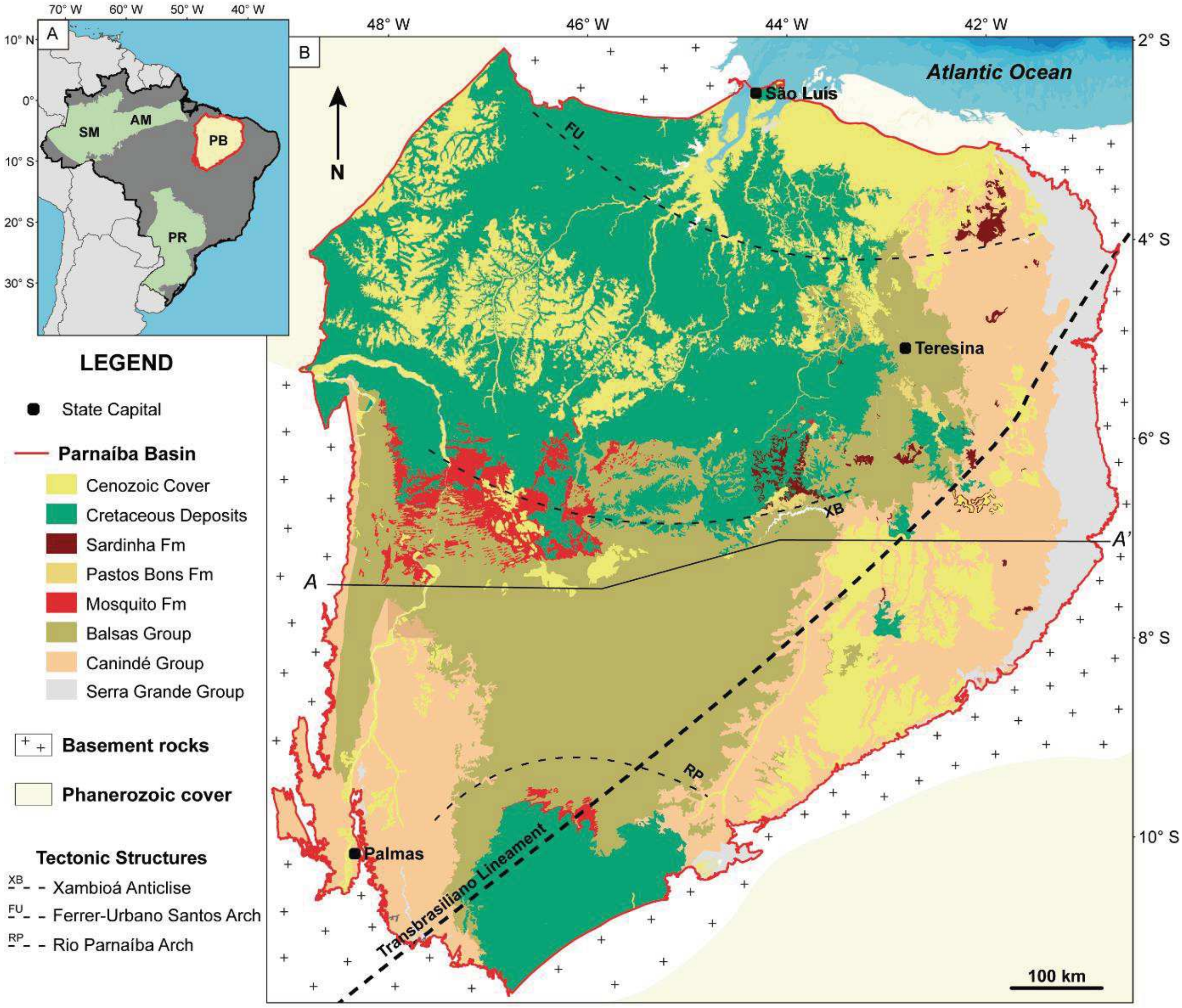

Figura 1. A) Bacias intracratônicas Paleozóicas do Brasil. B) Mapa da Bacia do Parnaíba dividido em unidades sedimentares e estruturas tectônicas. Base de dados extraída do banco de dados da CPRM, *Geobank* (CPRM, 2005).

A Supersequência Mesodevoniana-Eocarbonífera corresponde ao Grupo Canindé, constituído pelas formações Itaim, Pimenteiras, Cabeças, Longá e Poti, depositado de forma discordante sobre a supersequência anterior. Na base da sequência está a Formação Itaim, descrita como depósitos de tempestitos de ambiente de plataforma rasa. Acima, tem-se a Formação Pimenteiras, constituída de folhelhos escuros ricos em matéria orgânica. Durante a deposição dos folhelhos desta formação, diversos autores indicam o momento de transgressão máxima registrado na bacia. Após a ingressão marinha da Formação Pimenteiras está posicionada a Formação Cabeças, composta por diamictitos e arenito fino de ambiente nerítico plataformal com influência periglacial registrando um evento glacial no norte da América do Sul. A Formação Longá consiste de folhelhos laminados e siltitos bioturbados que sobrepõem a Formação Cabeças. Os depósitos desta formação são interpretados como registro de um ambiente deposicional de mar epicontinental, no qual os siltitos indicam a transgressão pós-glacial e os folhelhos, uma sedimentação mais profunda. No topo do grupo está a Formação Poti, constituída na base de arenitos finos e siltitos com estratificação cruzada *hummocky* interpretados como ambientes de deposição de *shoreface* inferior/superior marinho raso. No topo, arenitos com lentes de siltito interpretados como canais flúvio-estuarinos e planícies de maré (Figs. 2B, 2C e 2D) (GÓES e FEIJÓ, 1994; GÓES, 1995; MILANI e ZALÁN, 1999; VAZ et al., 2007).

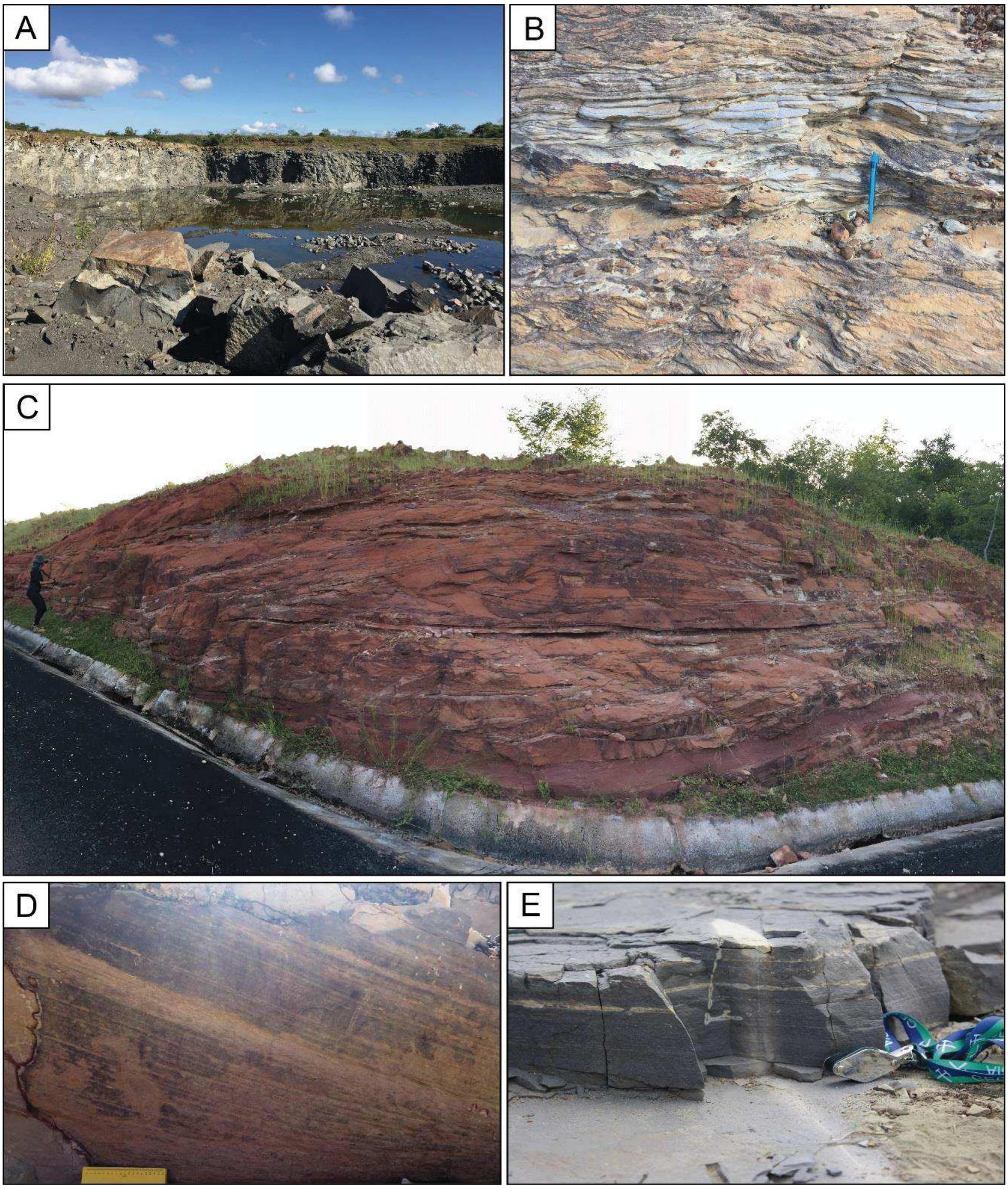

Figura 2. A) Pedreira próxima à cidade de Floriano-PI, afloramento da Formação Sardinha. B) *Climbing ripples* em arenitos da Formação Poti. C) Afloramento de arenito com estratificação cruzada *hummocky* da Formação Poti. D) Arenito com estratificação cruzada tangencial da Formação Poti. E) Siltito com intercalação centimétrica de arenito da Formação Pastos Bons.

Na Supersequência Mesodevoniana-Eocarbonífera estão contidos os principais sistemas petrolíferos da Bacia do Parnaíba em produção. No sistema Pimenteiras-Cabeças(!), os folhelhos marinhos radioativos da Formação Pimenteiras são as rochas geradoras com níveis máximos de até 6% de COT, enquanto os arenitos deltáicos da Formação Cabeças são as rochas reservatório. No sistema Pimenteiras-Poti(!), no qual a fonte geradora é a mesma, as rochas reservatório são os arenitos de ambiente costeiro da Formação Poti (ANP, 2015). Os folhelhos e seu caráter gerador estão diretamente relacionados aos pulsos intrusivos magmáticos na bacia que possibilitaram a maturação dos hidrocarbonetos pela ação térmica. Nos sistemas, as rochas ígneas atuam como *traps* estratigráficos em forma de soleiras e diques (RODRIGUES, 1995).

A Supersequência Neocarbonífera-Eotriássica é constituída pelo Grupo Balsas, formado pelas formações Piauí, Pedra de Fogo, Motuca e Sambaíba. Durante esta sequência a bacia sofre mudanças drásticas de ambiente deposicionais. Inicialmente desenvolveram-se mares abertos de clima temperado que passaram a mares restritos de clima árido, registrando contato concordante entre as formações. Um evento de regressão mundial no final do período Permiano causou uma progressiva desertificação do mar epicontinental da bacia, culminando na formação de depósitos desérticos relacionados à Formação Sambaíba. A presença de arenitos altamente ferruginosos da Formação Sambaíba indica a influência térmica de intrusões basálticas, sendo inferida uma contemporaneidade entre estes depósitos e os primeiros derrames dos basaltos da Formação Mosquito (VAZ et al., 2007; ARAÚJO et al., 2016; VIEIRA e SCHERER, 2017).

A Supersequência Jurássica é composta pela Formação Pastos Bons e teve sua subsidência inicial resultante de movimentos isostáticos decorrentes da carga das rochas intrusivas da Formação Mosquito e do pacote sedimentar. São depósitos de ambientes continentais associados a paleodepressões com contribuições fluviais em ambientes lacustres de clima árido (Fig. 2E). A fase final desta unidade sedimentar é consequente de movimentos tectônicos da abertura do Oceano Atlântico (VAZ et al., 2007; CARDOSO et al., 2017).

A Supersequência Cretácea está posicionada no topo do registro sedimentar da bacia. Em decorrência da abertura do Oceano Atlântico, o depocentro passou para a porção norte/nordeste, sendo as ingressões marinhas durante o período provenientes deste oceano. Esta sequência é constituída pelas formações Corda, Grajaú, Codó e Itapecuru (VAZ et al., 2007). Segundo Rossetti et al. (2001), as três primeiras formações são contemporâneas, indicado por interdigitações, e têm idades Neoaptianas a Eoalbianas. A Formação Itapecuru é interpretada como depósitos gerados em ambiente fluvial à estuarino/lagunar, em uma tendência transgressiva, discordantes sobre as formações Grajaú e Codó.

Durante o período Mesozóico, eventos distensivos de remobilização de falhas e surgimento de fraturas possibilitaram a intrusão de corpos ígneos na bacia. As intrusões se dividem em dois pulsos, as formações Mosquito e Sardinha, que ocorrem como diques e *sills* em toda a bacia. A Formação Mosquito é descrita por intrusões basálticas relacionados ao rifteamento do Atlântico Central e idades Eojurássicas, enquanto que a Formação Sardinha está associada a corpos basálticos dispostos principalmente em forma de diques, relacionados ao *rift* do Atlântico Sul e idades Eocretáceas (Fig. 2A) (BAKSI e ARCHIBALD, 1997; MERLE et al., 2011; SILVA et al., 2017).

A Formação Mosquito é correlacionada à Província Magmática do Atlântico Central (CAMP), um *Large Igneous Province* (LIP) que afetou termicamente rochas da América, Europa e África. O evento está associado a fragmentação do Supercontinente Pangeia que deu origem ao Oceano Atlântico Central. Neste contexto, a Formação Mosquito representa um conjunto de eventos intrusivos do CAMP, datado por Merle et al. (2011) utilizando Ar^{40}/Ar^{39} e obtendo idade de 199 ± 2,4 Ma. A Formação Sardinha é correlacionada a Província Magmática Paraná-Etendeka (PEMP), evento que afetou a América do Sul e África durante a abertura do Oceano Atlântico Sul. Diversos autores realizaram trabalhos de datação nas rochas desta formação, indicando idades entre ~120 e 130 Ma (FODOR et al., 1990; BAKSI e ARCHIBALD, 1997).

O MÉTODO TERMOCRONOLOGIA POR TRAÇOS DE FISSÃO

A Termocronologia por Traços de Fissão (TF) é atualmente um dos métodos termocronológicos mais usado para estabelecer histórias térmicas da crosta superior em diferentes ambientes tectônicos e geomorfológicos. O método TF proporciona informações de história térmica de baixa temperatura para apatita até ~120 ºC e para zircão até ~320 ºC. As idades derivadas do método são correlacionadas aos eventos térmicos aos quais uma amostra tenha sido submetida desde sua formação, e podem representar tanto a idade de cristalização da rocha, como a idade do(s) evento(s) térmico(s) (GALLAGHER et al., 1998; BERNET e GARVER, 2005; TAGAMI e O'SULLIVAN, 2005; LISKER et al., 2009).

O método se baseia na fissão espontânea dos átomos de ^{238}U contido no retículo cristalino dos minerais que causa a separação do isótopo de U em dois segmentos com forças repulsivas entre si, gerando traços iônicos nos trajetos da repulsão (traços de fissão). O método TF é aplicado a minerais acessórios cuja concentração de ^{238}U (1-1000 ppm) seja suficiente para contagem/medição dos traços, sendo os mais comuns a apatita, o zircão e a titanita. Os traços recém-formados possuem comprimento médio de ~11 μm (zircão) e ~16 μm (apatita). Estes traços são continuamente produzidos no mineral ao longo do tempo, podendo ser observados em microscópio óptico sob aumentos de aproximadamente 1200x, depois de um ataque químico conveniente. O processo de fissão que danifica o cristal produzindo os traços é termicamente ativado, sendo iniciado na temperatura de fechamento para cada mineral. Acima da temperatura de fechamento, os traços se remobilizam e tendem a se apagar (GALLAGHER et al., 1998; KETCHAM et al., 1999; BERNET e GARVER, 2005; REINERS e BRANDON, 2006).

Segundo Dodson (1973), a temperatura de fechamento é definida como a temperatura de um dado termocronômetro (p.ex., TF em zircão ou apatita) no momento correspondente à sua idade aparente (p.ex., idade TF). Em apatitas, esta temperatura é fortemente influenciada pela composição química dos cristais, e no zircão ao dano acumulado de radiação no cristal (metamictização). Diversos experimentos realizados por diferentes pesquisadores (GALLAGHER et al., 1998; KETCHAM et al., 1999) indicam temperaturas de fechamento genéricas para as apatitas, variando de 60 °C a 120 °C, sendo que as flúor-apatitas possuem temperaturas de fechamento menores, enquanto que as cloro-apatitas temperaturas maiores. A determinação composicional das apatitas, o teor de cloro, pode ser realizada por microssonda eletrônica, e pela determinação do Dpar. O Dpar é a medida do diâmetro paralelo ao eixo cristalográfico "c" do traço em um cristal, formado pela intersecção de um *etch pit* com a superfície polida do cristal (DONELICK, 1993). O Dpar indica correlação positiva com teores de Cl e OH, e negativa com F, sendo possível identificar a composição da apatita analisada, a partir de sua medida. No zircão, cristais com maiores danos de radiação possuem temperaturas de fechamento mais baixas (~180–260 °C) e são menos resistentes ao apagamento dos traços do que cristais com menos danos (300–360 °C) (GALLAGHER et al., 1998; GARVER et al. 2005; REINERS e BRANDON, 2006).

Outro conceito importante no método TF é o processo de encurtamento e apagamento dos traços que ocorre em uma escala de temperatura chamada de Zona de *Annealing* Parcial (PAZ) (WAGNER, 1979). Esta zona compreende temperaturas de 60 °C a 120 °C nas apatitas e 180 °C a 320 °C no zircão. Nesta zona, novos traços começam a ser formados e os antigos encurtados, porém todos os traços sofrem um contínuo encurtamento se permanecerem nesta zona por um certo período. Segundo Laslett et al. (1987), o tempo necessário para alterar o comprimento dos traços é de ~10 Ma para fontes térmicas monotônicas, podendo variar para fontes de calor heterogêneas. Se o cristal for aquecido além desta zona de temperatura (p.ex. T>120 °C em apatitas) pode sofrer o *annealing* total dos traços, redefinindo a estrutura cristalina. Dessa forma, a temperatura de fechamento (máxima) se torna um limiar importante na história térmica do mineral, por ser o início da geração dos traços e à ela é indicada uma idade aparente. Em altas temperaturas, os cristais adquirem energia suficiente para recuperar a estrutura cristalina e "apagar" os traços, perdendo a capacidade de armazenar os dados de história térmica (GALLAGHER et al., 1998; DONELICK et al., 2005; TAGAMI, 2005).

Idades TF em Apatita e Zircão

O cálculo da idade TF é atribuído, genericamente, à estimativa da densidade de traços espontâneos no mineral oriundos do isótopo-pai (^{238}U) e da densidade dos traços de fissão induzidos na mica, sendo necessária uma correta correlação entre as duas áreas (mineral e mica) para uma idade traço de fissão precisa. Por meio do método do detector externo, no qual as amostras são irradiadas em contato com as micas, os dados são gerados para cada cristal e compõem parâmetros para o cálculo. Este cálculo é realizado pela fórmula abaixo:

$$t = \frac{1}{\lambda_d} ln\left(\lambda_d \frac{\rho_s}{\rho_i} \rho_d \zeta g + 1\right)$$

Onde, t é a idade; ρ_s e ρ_i são os traços espontâneos e induzidos contados em uma unidade de área; λ_d é a constante de decaimento de U^{238} (4,47 x 10^9 anos); ρ_d é a densidade de traços no dosímetro posicionado junto com as amostras na irradiação; g é o fator de eficiência relacionado ao detector externo (0,5); e ζ é a constante de calibração do responsável técnico pela contagem. A calibração ζ é determinada empiricamente pela contagem de traços em um padrão (e.g. Apatita de Durango, Zircão Fish Canyon Tuff), ou seja, amostras que possuem comportamento homogêneo e idades bem estabelecidas (HURFORD e GREEN, 1983). Dessa forma, a presença da calibração na fórmula busca um caráter homogêneo ao resultado, independentemente do responsável que realiza a contagem (GALLAGHER et al., 1998, DONELICK et al., 2005).

As idades traços de fissão são constituídas por uma média estimada de idade de uma população de grãos individuais de cada amostra. Tipicamente são datados 20 (amostras do embasamento) a 30 (amostras detríticas) grãos para uma amostra (GALLAGHER et al., 1998). Antes de ser realizado o cálculo da média é realizado o teste χ^2, o qual identifica a homogeneidade das idades dos grãos. Resultados de $\chi^2>5$ indicam uma população de idade, enquanto que resultados de $\chi^2<5$ e dispersão>15% indicam mais populações. Assim, quando há mais de uma população, os conjuntos são analisados separadamente e compostas médias diferentes para cada população, identificam eventos térmicos distintos. Estatisticamente, as idades podem ser calculadas de três formas: média, *pooled* e central. A idade média é a simples média aritmética da razão de traços espontâneos e induzidos, enquanto a idade *pooled* é a divisão da quantidade total de traços espontâneos e induzidos. A idade central é a média ponderada com distribuição logarítmica normal de uma população de grãos. De maneira geral, amostras de rochas exumadas rapidamente possuem idades homogêneas com médias semelhantes, por outro lado, amostras detríticas podem conter idades não concordantes, contendo informações de diferentes eventos de exumação (GALBRAITH e LASLETT, 1993; GALLAGHER et al., 1998; DONELICK et al., 2005).

Aplicação do Método TF

O método TF possui diversas aplicações e resulta em diferentes dados térmicos passíveis de interpretação para o contexto de uma área de estudo. Diferentes regiões possuem particularidades que podem afetar ou não os termocronômetros, sendo uma questão de magnitude e duração da fonte de calor. Estas particularidades são os diferentes processos que podem influenciar no aumento ou diminuição de temperatura como soterramento, falhas, intrusões e soerguimento. Neste sentido, os dados resultantes do método indicam condições de tempo e temperatura, cabendo ao analista interpretar estes dados, correlacionando com os processos em uma dada área de estudo. Em bacias sedimentares, estes métodos corroboram para interpretações combinadas com técnicas de modelagem possibilitando a avaliação de: (a) processos de formação da bacia, taxas de soterramento; (b) deformação; (c) datação e duração da geração, migração e *trap* de hidrocarbonetos; (d) efeitos de intrusões e fluidização na bacia;

e (e) alterações climáticas passadas (GALLAGHER et al., 1998; ARMSTRONG, 2005; REINERS e BRANDON, 2006).

Em bacias sedimentares, o método TF vem sendo amplamente aplicado na estruturação de histórias termais para sistemas petrolíferos. Nos estudos, são identificados picos de máxima paleotemperatura a fim de contextualizar os estágios/duração de maturação dos hidrocarbonetos. Estudos como de Osadetz et al. (2002) e Tingate e Duddy (2002) identificam possíveis eventos térmicos por TF em apatita de maturação de hidrocarbonetos em períodos do fim do Paleozóico e no Mesozóico para as bacias sedimentares de Williston (Canadá) e Officer (Austrália), respectivamente. Na Cordilheira dos Andes, Mora et al. (2010) desenvolveram um estudo no qual são propostos modelos de deformação baseados em idades de TF em apatita e zircão que estão diretamente relacionados aos sistemas petrolíferos das bacias do leste andino.

THERMAL HISTORY OF POTENTIAL GAS RESERVOIR ROCKS IN THE EASTERN PARNAÍBA BASIN, BRAZIL

Márcio Cardoso Jr.[a]*; Farid Chemale Jr.[a]; Christie H. Engelmann de Oliveira[a]; Carlos Emanoel de Souza Cruz[b]; Carlos Jorge de Abreu[b]; Frederico Antonio Genezini[c]

[a] *Programa de Pós-Graduação em Geologia, Universidade do Vale do Rio dos Sinos, 93022-000 São Leopoldo, RS, Brazil*

[b] *Instituto de Geociências, Universidade de Brasília, 70910-900 Brasília, DF, Brazil*

[c] *Instituto de Pesquisas Energéticas e Nucleares - IPEN-CNEN, São Paulo, SP, Brazil*

*Corresponding author. *Email address*: marciocard@edu.unisinos.br

Abstract:

The Parnaíba Basin is a major intracratonic sedimentary basin in Brazil and its natural gas systems are a potential natural resource formed by the influence of igneous intrusions. To constrain the thermal history of unexplored potential reservoir rocks in the eastern part of the Parnaíba Basin, sedimentary rocks near intrusions were analyzed by petrography and thermochronology (apatite and zircon fission track: AFT and ZFT). Petrography shows dissolutions and carbonate clays pore filling generated by thermal destabilization of feldspars and overburden of intrusions. AFT results indicate high partial annealing by the last magmatic event in the basin, and ZFT results show ages of maximum paleotemperature compatible with the Sardinha magmatic event. In the thermal history models, rocks closed to the intrusion were influenced and underwent maximum paleotemperatures above 300 °C (572 °F), which is higher than the favorable conditions for reservoir rocks. As a result of these temperatures, hydrothermal fluid modified the diagenetic evolution of the succession by dissolving and precipitating carbonate cement in pore space. In the studied area, at distances greater than 50 m

(164 ft) from the intrusion the rocks were not be altered to be appropriated to a reservoir context in terms of paleotemperature. This study includes an innovative approach for thermochronological data in the analysis of thermal histories of petroleum systems.

Keywords: Fission-tracks; Basic Sills; Petroleum systems; Parnaíba Basin; CAMP Magmatism; Northeastern Brazil.

1 INTRODUCTION

Petroleum systems occur in a variety of geological contexts and require some factors to generate and preserve hydrocarbons. Physical and thermo-chemical factors control the right conditions for natural production and accumulation. Physical factors of petroleum systems involve organic carbon matter accumulation, followed by hydrocarbon migration and retention under trapping and sealing settings. The thermo-chemical factors are also important conditions that change rock properties, conducing organic matter to stages of hydrocarbon maturation. Some maturation stages can only be achieved as result of increasing temperature (e.g. burial, faulting, magmatic intrusion) in sedimentary basin evolution (Magoon and Dow, 1994; Welte et al., 2012).

Distinct types of sedimentary basins have thermal behaviors linked to tectonic settings. During basin evolution, different tectonic events can occur caused by extensional or compressional forces and resulting in basin subsidence or uplift. These events change thermal behavior of basins by modifying geothermal gradient of the upper crust that interferes in petroleum systems (Allen and Allen, 2013). Usually, burial is the primary mechanism that increases temperature and contributes to hydrocarbon generation in thick basins, whereas shallow depth basins need other events to naturally achieve hydrocarbon maturation temperatures. Intrusive magmatic activity is a prime example of temperature shift in the thermal history of a sedimentary basin and contributes in many ways to form a petroleum system.

Several petroleum systems in sedimentary basins are currently in exploration based on igneous intrusion models (e.g., North Atlantic and Australia; see more in Senger et al., 2017). However, intrusions can also affect diverse elements and processes (migration, reservoir, trap and seal) in these systems in either positive or negative ways according to the magnitude and/or placement of magmatism. The understanding of the thermal factors can lead to prediction models to target promising areas for hydrocarbon resources (Poelchau et al., 1997; Yalçin et al., 1997).

In the Paleozoic, several sedimentary basins started to develop in Gondwana supercontinent. In the western part of the supercontinent, the Parnaíba, Congo, Paraná and Cape-Karoo basins cover large areas and show similarities in their intracratonic genesis and depositional histories (Linol et al., 2016). They have complex post-depositional thermal histories associated to tectonic processes of Gondwana. In the north, the basins had extensional movements resulting in the opening of Central and North Atlantic Ocean. These movements triggered subvolcanic magmatism named Central Atlantic Magmatic Province (CAMP) (e.g., Marzoli et al., 1999; Mizusaki et al., 2002; Nomade et al., 2007) that extensively intruded cratonic areas and sedimentary basins in the Jurassic, and recorded in thermochronological ages as shown by Dias et al. (2017) in the Araguaia Belt, Brazil. In the south, the extensional context led to the Paraná-Etendeka magmatism emplacement during Cretaceous that thermally affected the Brazilian margin (e.g., Engelmann de Oliveira et al., 2016). Some of the magmatic events influenced petroleum systems of the Paleozoic intracratonic basins of Gondwana (Brown et al., 1994; Milani and Zalán, 1999; Zalán, 2004; Burke et al., 2003; Thomaz Filho et al., 2008).

In the Parnaíba Basin, the magmatic activity thermally affected the rocks of late Devonian petroleum systems (Rodrigues, 1995). The basin has sedimentary layers nearly horizontal and continuous, which were intruded during the Mesozoic by igneous rocks divided in two major magmatic events (Mosquito and Sardinha Formations). These events are associated to CAMP and Paraná-Etendeka magmatism and occur as sills and dykes between different sedimentary strata. Intrusions acted in the thermal maturation of the source rock, migration enhancement and stratigraphic trapping, and sealing reservoir rocks. In these settings, the reservoir layers were altered by late intrusions and have irregular shapes, controlled by placement and heat exchange with the igneous intrusions (Kingston and Matzko, 1995; Porto and Pereira, 2014; Miranda et al., 2016).

The Parnaíba Basin is the fourth most productive of natural gas in Brazil (ANP, 2017). According to the Brazilian National Petroleum Agency (ANP), the exploration in the Parnaíba Basin in 2017 was ca. 5,700 Mm^3/day. Its main petroleum systems comprise the Pimenteiras Formation as source rock and the Cabeças and Poti Formation as main reservoir (Cunha et al., 2012). These systems are directly correlated to the magmatic intrusions that acted in thermal maturation as well as stratigraphic and structural trapping (Rodrigues, 1995; ANP, 2015). Application of apatite fission-track (AFT) and zircon fission-track (ZFT) analyses in hydrocarbon exploration are well-established methods that allow paleotemperature determination in the ca. 60-120 °C (140-248 °F) and ca. 180-320 °C (284-608 °F) ranges (e.g. Bernet and Garver, 2005; Donelick et al., 2005). These analyses are widely used to constrain the thermal history of the upper crust and provide constraints on the timing and duration of heating and cooling events in sedimentary basins (e.g. Green et al., 2004; Engelmann de Oliveira et al., 2016). The ZFT method is particularly useful because the temperature range is comparable to the gas maturation stage (>200 ºC (392 °F)); gas is largely exploited in the Parnaíba Basin.

In this study, an integrated approach combines petrography, AFT and ZFT analyses applied to understanding the influence of igneous rocks in paleotemperature. Also, information is obtained on the thermal history of potential reservoir rocks in the eastern part of the Parnaíba Basin, where sedimentary and igneous bodies occur closely placed. For this purpose, outcrop and borehole samples were analyzed to delimit the thermal history of the rocks and to evidence the alteration of reservoir layers. Results show that rocks closer to the intrusion underwent maximum paleotemperatures above favourable conditions for reservoir rocks. Rocks farther from the intrusion have better reservoir characteristics in terms of paleotemperature. The results expand the use of thermochronological methodology in detrital sedimentary rocks and is proposed as an alternative way to constrain thermal histories in rocks with low or no organic material.

2 GEOLOGICAL SETTING

The Parnaíba Basin is an intracratonic sedimentary basin which covers ca. 600,000 km² (231,661 mi²) of northeastern Brazil (Fig. 1A and 1B) and has a 3.5 km (2.17 mi) thick volcanic-sedimentary record with a long Phanerozoic depositional history (e.g., Góes and Feijó, 1994; Vaz et al., 2007). The basin covers an amalgamation of different Precambrian terranes generated during the Brasiliano orogeny (Brito Neves, 2002). Basement rocks of the basin are divided into: (a) Parnaíba Block in a totally covered central area showing featureless reflector patterns and interpreted as granitic terrane (Daly et al., 2014); (b) basin edges partially covering cratonic areas (Amazonas, São Luís and São Francisco cratons) and mobile belts (Gurupi Belt, and Borborema and Tocantins provinces) which are distinct blocks and suture zones juxtaposed during the Brasiliano orogeny (de Castro et al., 2014).

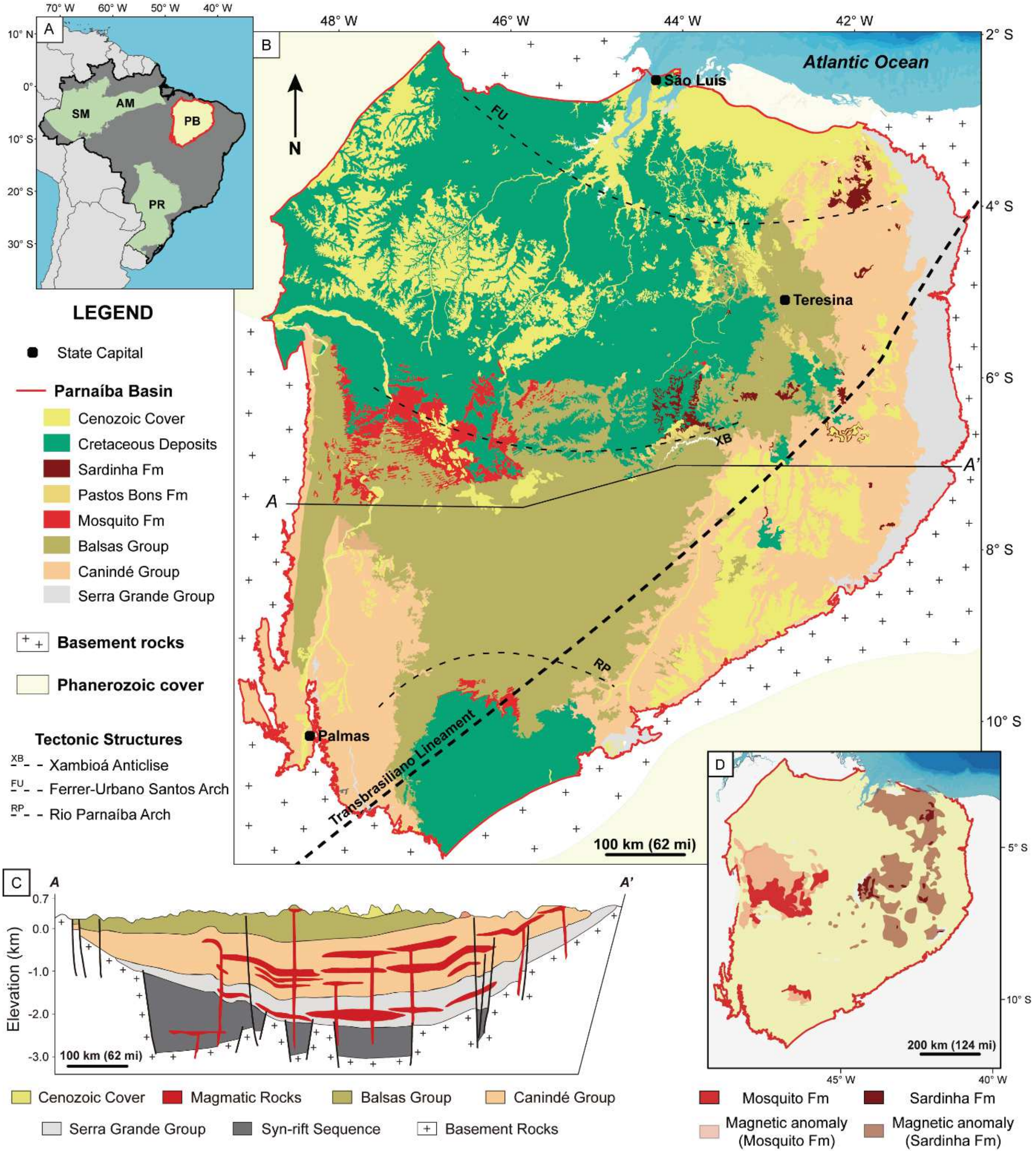

Figure 1. A) Location map. Brazilian Paleozoic intracratonic basins, SM – Solimões Basin; AM – Amazonas Basin; PB – Parnaíba Basin; and PR – Paraná Basin. B) Parnaíba Basin divided in sedimentary units and major tectonic structures. C) Schematic cross-section of the Parnaíba Basin (modified from Góes et al., 1990). D) Interpretative geophysical map of the magnetic anomalies of Mosquito and Sardinha Formations (modified from Mocitaiba et al., 2017).

In the early Cambrian to Ordovician, lithospheric stretching of Western Gondwana and Laurentia resulted in reactivation of a rift system along preexisting weakness zones in the basement rocks. The stretching formed NE- to E-W-oriented grabens along the Transbrasiliano Lineament which initiated the formation of rift basins, such as the Jaibaras Trough covered by sedimentary rocks (Oliveira and Mohriak, 2003). These early Paleozoic grabens were filled by fluvial-lacustrine sediments of the pre-syneclise stage of Parnaíba Basin (Almeida and Carneiro, 2004). The initial subsidence of the late Parnaíba Basin sag stage is explained as result of thermal subsidence (lithospheric contraction) during Ordovician to Silurian. From the initial subsidence until the early Carboniferous, the principal depositional axis of the basin was over the Transbrasiliano Lineament on the eastern edge (Oliveira and Mohriak, 2003; Daly et al., 2014; de Castro et al., 2016).

The sedimentary infill of the Parnaíba Basin is divided into five supersequences bounded by major unconformities (Fig. 2A): Silurian, Middle Devonian-Lower Carboniferous, Upper Carboniferous-Lower Triassic, Jurassic and Cretaceous (i.e., Vaz et al., 2007). The Silurian supersequence corresponds to a 2nd order transgressive-regressive cycle. It covers the basement and has sandstones and siltstones. This supersequence corresponds to the Serra Grande Group described by Della Fávera (1990), Góes and Feijó (1994) and Góes (1995).

The Middle Devonian-Lower Carboniferous Supersequence lies above the supersequence and is equivalent to the Canindé Group. The group includes sandstones and mudstones of the Itaim, Pimenteiras, Cabeças, Longá and Poti Formations. The Itaim Formation is described as shallow marine, storm-dominated sandstone. The Pimenteiras Formation is characterized by fine-grained rocks and includes organic-rich black shales, which correspond to the maximum flooding stage of this supersequence as well as the entire depositional history of the Parnaíba Basin. The Cabeças Formation is composed of glacial-influenced, shallow marine sandstones. The Longá Formation includes sandstone and siltstone deposited in similar conditions as the Itaim Formation. In addition, the uppermost Poti Formation has sandstones related to transitional environments (upper shoreface, estuarine and fluvial-estuarine) (Góes and Feijó, 1994; Góes, 1995; Milani and Zalán, 1999; Vaz et al., 2007).

In the late Carboniferous, Pangea aggregation started to compress and uplift some areas such as the Ferrer-Urbano Santos and Rio Parnaíba arches, moving the basin depocenter towards the west (Xambioa anticlise) and delimiting the contour of the Parnaíba Basin. The Upper Carboniferous-Lower Triassic Supersequence is related to a drastic climate change, when open seas of temperate climate became restricted due to global sea-level fall (Becker, 1993). During this period, a progressive desertification occurred in the basin with deposition in arid environment. This supersequence is also called Balsas Group and was majorly dominated by continental and restricted marine depositional settings (e.g. Araújo et al., 2016; Vieira and Scherer, 2017). Extensional movements related to Pangea rupturing caused the intrusion of sills and dykes with Jurassic (Mosquito Formation) and Cretaceous age (Sardinha Formation) (Fig. 1C and 1D) (Fodor et al., 1990; Silva et al., 2017).

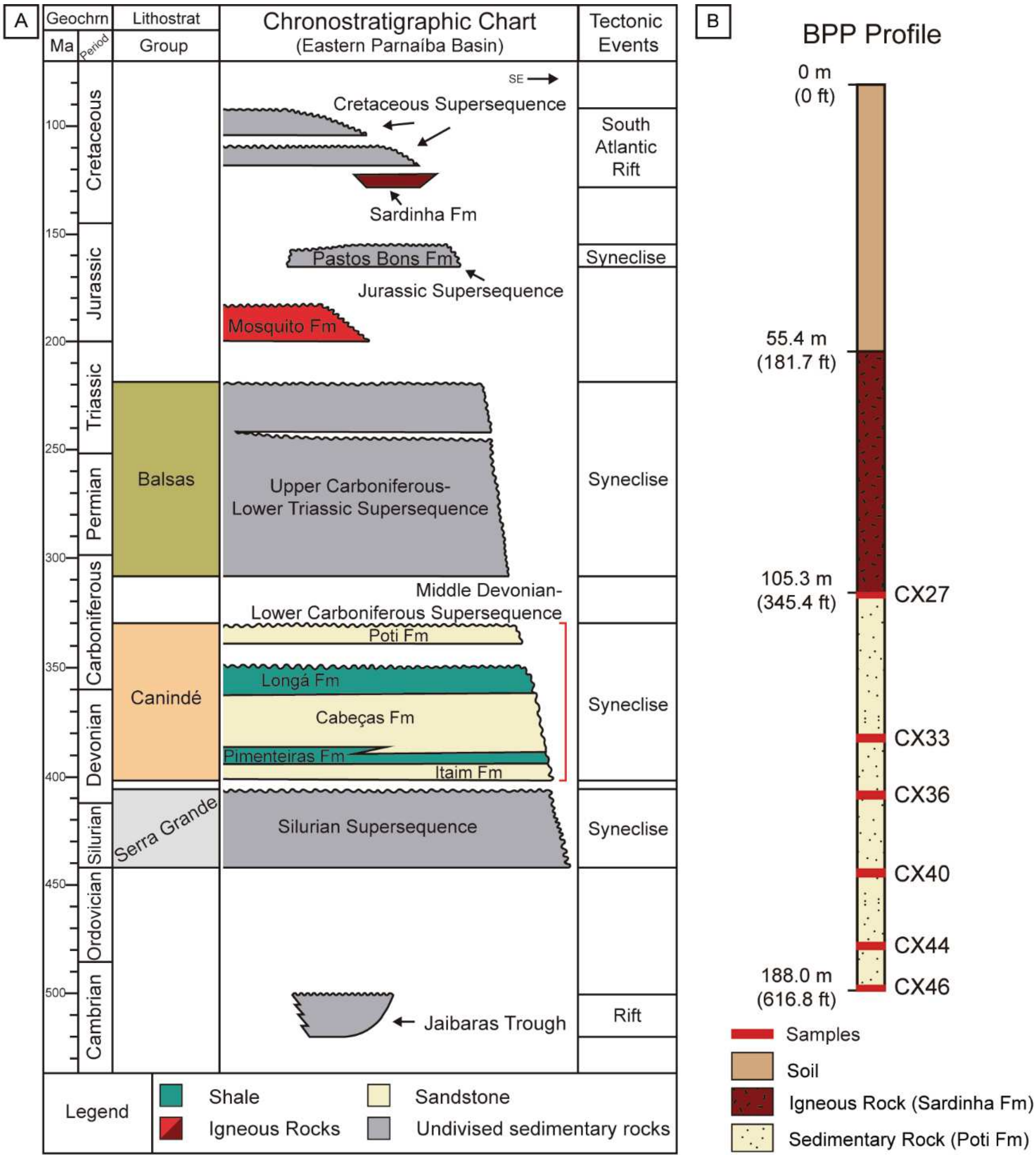

Figure 2. A) Chronostratigraphic chart of eastern Parnaíba Basin (modified from Vaz et al., 2007). B) Schematic profile of BPP borehole. Red marks highlight position of collected samples.

Mosquito Formation is composed of basaltic dykes and sills associated with the early North and Central Atlantic Ocean rift (~200 Ma) (Merle et al., 2011) and the Penatecaua magmatism in the Amazonas Basin as part of CAMP (Marzoli et al., 1999). The Jurassic supersequence is formed by the Pastos Bons Formation, whose sediments were deposited in continental environments in low areas due to magmatic overload of the Mosquito Formation.

During the Cretaceous, the South Atlantic Ocean rift caused major marine ingressions changing depositional systems. Rifting movements along with Pangea break-up generated a new intrusion, the Sardinha Formation, formed by dykes with early Cretaceous age (120-130 Ma) (Fodor et al., 1990; Baksi and Archibald, 1997) and associated with magmatism of the Serra Geral Group in the Paraná Basin (Thomaz Filho et al., 2000). The final supersequence is Cretaceous, deposited in continental to transitional marine environments (aeolian and fluvial-lacustrine to shallow platform) with the depocenter located in the northwestern part of the basin, and composed by the Corda, Grajaú, Codó and Itapecuru Formations.

3 MATERIALS AND METHODS

Samples from four outcrops and six boreholes were collected in Parnaíba Basin from the Cabeças, Poti, Pastos Bons and Corda Formations in portions near intrusions (less than 40 m (131 ft), except sample PA06). More details of each sample are provided in Table 1 and Figures 2B and 3.

Table 1. Details of samples studied with fission-tracks and petrography

Sample	Lithology/ Formation	Latitude	Longitude	Elevation/Depth (m)	Stratigraphic Age (Ma)	AFT	ZFT	Petrography
Borehole BPP								
CX27	Sandstone/ Poti	42° 19' 22"	06° 30' 07"	- / 105.3 – 106.3	331 - 339	X	X	X
CX33	Sandstone/ Poti	42° 19' 22"	06° 30' 07"	- / 134.9 – 136.3	331 – 339	X	X	X
CX36	Sandstone/ Poti	42° 19' 22"	06° 30' 07"	- / 146.9 – 148.3	331 – 339	X	X	X
CX40	Sandstone/ Poti	42° 19' 22"	06° 30' 07"	- / 163.0 – 164.5	331 – 339	X	X	X
CX44	Sandstone/ Poti	42° 19' 22"	06° 30' 07"	- / 178.2 – 179.5	331 – 339	X	X	X
CX46	Sandstone/ Poti	42° 19' 22"	06° 30' 07"	- / 187.1 – 188.0	331 – 339	X	X	X
Outcrop								
PA02B	Sandstone/ Corda	42° 57' 12"	06° 48' 08"	135 / -	111 - 119	X	X	X
PA03A	Siltstone/ Pastos Bons	42° 57' 06"	06° 48' 30"	146 / -	154 - 165	X	X	X
PA06	Siltstone/ Poti	43° 11' 26"	06° 42' 18"	121 / -	331 – 339		X	
PA09A	Sandstone/ Cabeças	41° 34' 34"	07° 01' 58"	274 / -	364 - 390	X	X	X

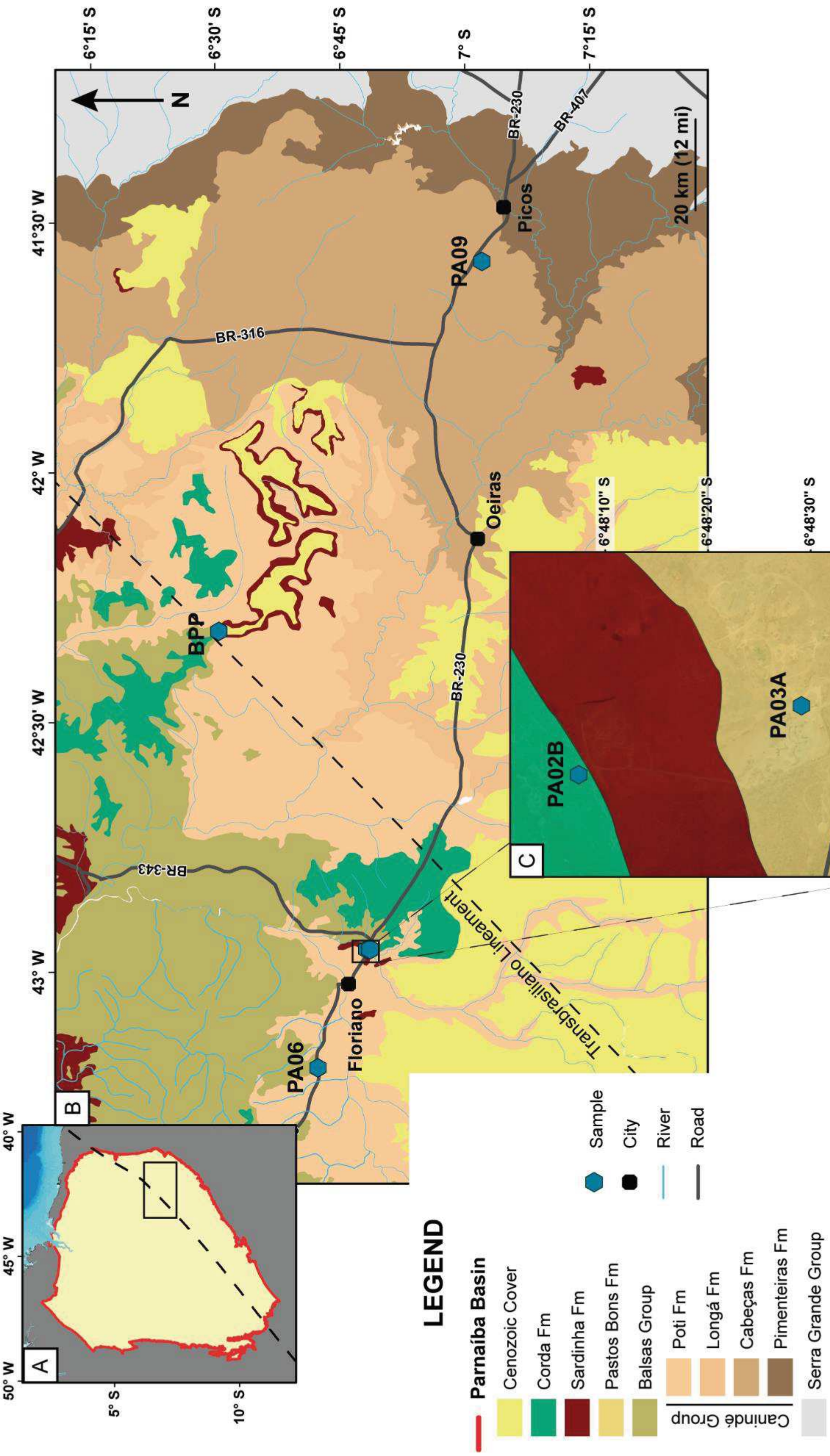

Figure 3. Geologic map of the study area. A) Parnaíba Basin and the Transbrasiliano Lineament. B) Study area. Borehole BPP and sample location. C) Location of samples PA02B and PA03A.

3.1 Petrography

Petrographic analysis was performed in three outcrop samples and all six borehole samples. These samples were selected to study petrographic aspects of the interaction between intrusions and sedimentary rocks. The depositional and diagenetic study included thin sections of samples under the optical polarizing microscope Zeiss AXIO Lab.A1 with 2.5x, 10x, 20x, 50x objectives, at Universidade do Vale do Rio dos Sinos, Brazil. Petrographic information can be found in Table 2. Standard point counting technique (Dickinson et al., 1983) was used to distinguish different components of the sedimentary rocks.

3.2 Thermochronology

AFT and ZFT thermochronology were performed in all samples (Table 1). Apatite and zircon grains were concentrated using conventional methods of crushing and magnetic, heavy liquid and hand-picking separation. Apatite grains were mounted in epoxy resin, polished and etched for 20 s in a 5.5 M HNO_3 solution at 21 °C (69.8 °F) to reveal the fission tracks. Zircon grains were mounted in Teflon®, polished and etched in a NaOH-KOH melt solution at 230 °C (446 °F). We adopted the multi-mount technique and prepared two or three zircon mounts per sample (Bernet and Garver, 2005), etched for different periods of time varying from 3 to 14 h. The mounts were covered with low-U mica sheets and dated by the external detector method (Hurford, 1990). Neutron irradiation was done in the IPEN-CNEN Reactor, São Paulo, Brazil, using CN2 dosimeter glasses, Durango age standard for apatite mounts, and Fish Canyon Tuff age standard for zircon mounts.

AFT and ZFT analyses were performed at the Low-Temperature Thermochronology Lab at Universidade de São Paulo, Brazil, using an Olympus BX51 Microscope (1250x, dry) with a digitalizing tablet and a computer-controlled stage drive by the FTStage 4.05 software (Dumitru, 1993). For each sample, 20 grains or more were dated counting both thermochronometers. A summary of AFT and ZFT data is shown in Table 4. AFT and ZFT ages and errors were calculated following the zeta-calibration (ζ) method (Hurford and Green, 1983) with the RadialPlotter software (Vermeesch, 2009). A zeta-calibration factor of 135.4 ± 2.6 (CN2; C. Engelmann de Oliveira) was used. Fission tracks age errors are quoted at 1σ confidence level and derived by conventional method (Green, 1981). The Chi-squared test (χ^2) was used to quantify individual ages of a unique population, in which a χ^2>5% is considered to represent a concordant age so samples contain a single age population (Galbraith and Laslett, 1993). AFT lengths were measured on horizontal confined fission tracks. Etch pit diameter (Dpar; Donelick et al., 2005) values were used as a kinetic parameter.

Thermal modeling was performed using the HeFTy v. 1.9.3 software (Ketcham, 2005). Input data include AFT and ZFT fission track ages, track lengths when available, and Dpar as a kinetic parameter. We used the kinetic annealing model of Ketcham et al. (2007) for AFT and Rahn et al. (2004) for ZFT. The inversion modeling was run until 100 good models (Goodness of Fitness, GOF > 0.5) were obtained (Ketcham, 2005) using a Monte-Carlo search method. Stratigraphic ages and present-day temperature were included as constraints allowing the software to search for a wide range of a coherent time-temperature (t-T) spectra. Additional constraining boxes delimitate the intrusion age of the Mosquito and Sardinha Formations; ages of the youngest unconformities of the basin (125-120 Ma and 110-105 Ma) were included for thermal modeling of the samples.

4 RESULTS

4.1. Petrography

Poti Formation samples from the borehole (CXs samples) are mostly composed of mono- and polycrystalline quartz (>85 vol.%); plagioclase and K-feldspar are present in minor proportion (Table 3) and rock fragments are rare. According to Dickinson et al. (1983) diagram, these samples are derived from intracratonic sources (Fig. 4). Samples are sandstones, grain-supported and long compaction contacts between grains. Other petrographic information can be found in Table 2. In the borehole samples, two major groups show different depositional and diagenetic features. The upper group (CX27, CX33 and CX36) has bimodal grain distribution of two average grain sizes in thin section (Fig. 5C). The lower group (CX40, CX44 and CX46) has smaller grain size and high sphericity compared to the upper group (Fig. 5E).

The upper group is cemented by kaolinite and chalcedony, and grain dissolution resulted from eodiagenesis (Fig. 5A). The lower group has similar cement in the pore spaces but different diagenetic composition from initial process of illitic clays (illite and smectite) formation from micas and presence of small, nearly cubic crystals of pyrite (Fig. 5D).

Table 2. Selected petrographic information

Sample	Average Size (mm)	Sorting	Rounding	Sphericity	Compaction Grain contacts	Matrix
Poti Formation						
CX27	0.7/0.3	Moderate	Sub-rounded to rounded	Low	Long	None
CX33	1.5/0.2	Moderate	Sub-rounded to rounded	Low	Long	None
CX36	1/0.5	Moderate	Sub-rounded to rounded	Low	Long	None
CX40	0.3	Well	Sub-rounded to rounded	High	Long	None
CX44	0.3	Well	Sub-rounded to rounded	High	Long	None
CX46	0.2	Well	Sub-rounded to rounded	High	Long	None
Corda Formation						
PA02B	0.3	Well	Sub-rounded	Low	Long	None
Pastos Bons Formation						
PA03A	>0.1	Well	Rounded	High	-	Fe-oxides
Cabeças Formation						
PA09A	0.5	Moderate	Sub-angular to sub-rounded	Low	Point to Long	None

All information was visually determined in the majority of grains and contacts in thin sections during point counting.

Porosity differentiates the two groups, but primary porosity was not found in any sample. Primary porosity is occluded as result of compaction and post-depositional cementation (Fig. 5B). Following standard 300-point counting, samples showed secondary porosity from grain and cement dissolution. In the borehole samples, the upper group has higher porosity than the lower group (Figs. 5B and 5F).

Table 3. Modal composition

Sample	Monoquartz/ Polyquartz	Feldspar	Rock Fragments	Cement	Porosity	Others	Total
Poti Formation							
CX27	58/13	1	1	18	9	-	100
CX33	50/12	1	3	15	19	-	100
CX36	57/17	3	-	10	12	1	100
CX40	61/15	7	1	4	2	5	100
CX44	62/13	8	2	9	3	3	100
CX46	52/18	9	1	14	5	1	100
Corda Formation							
PA02B	50/8	8	2	14	17	1	100
Cabeças Formation							
PA09A	50/9	-	1	12	28	-	100

Results are in percent based on point counting in each sample. Feldspar includes K-feldspar and plagioclase. Cement is kaolinite, quartz or ferruginous minerals. Porosity is secondary. Other minerals are zircon, mica and Fe-oxides.

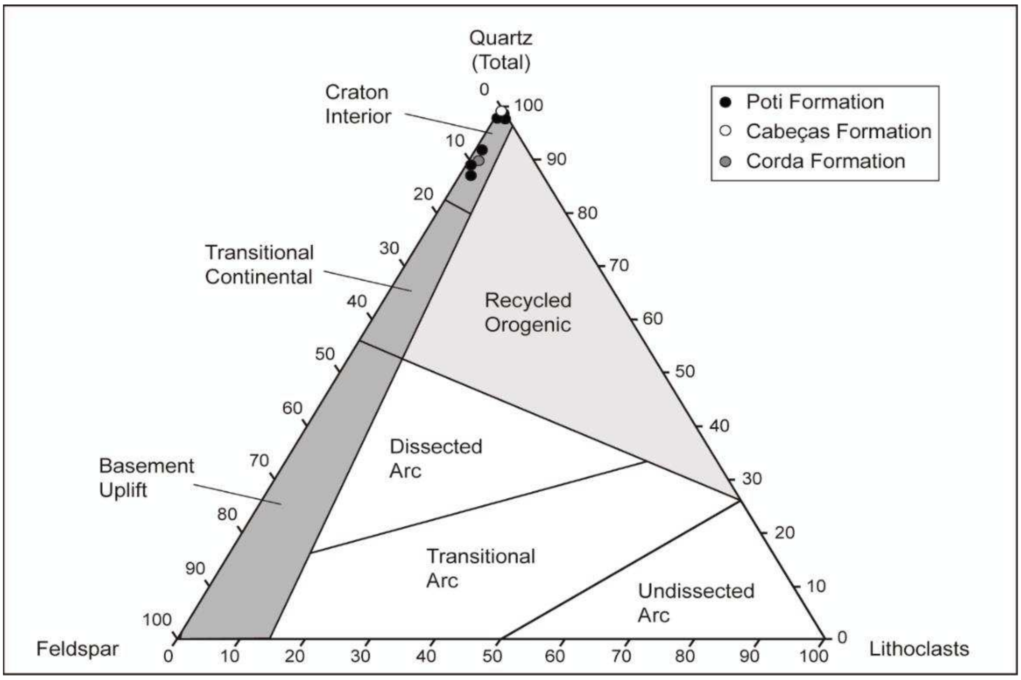

Figure 4. Sandstone provenance diagram (Dickinson et al., 1983) indicates quartzose recycled sources from craton interior.

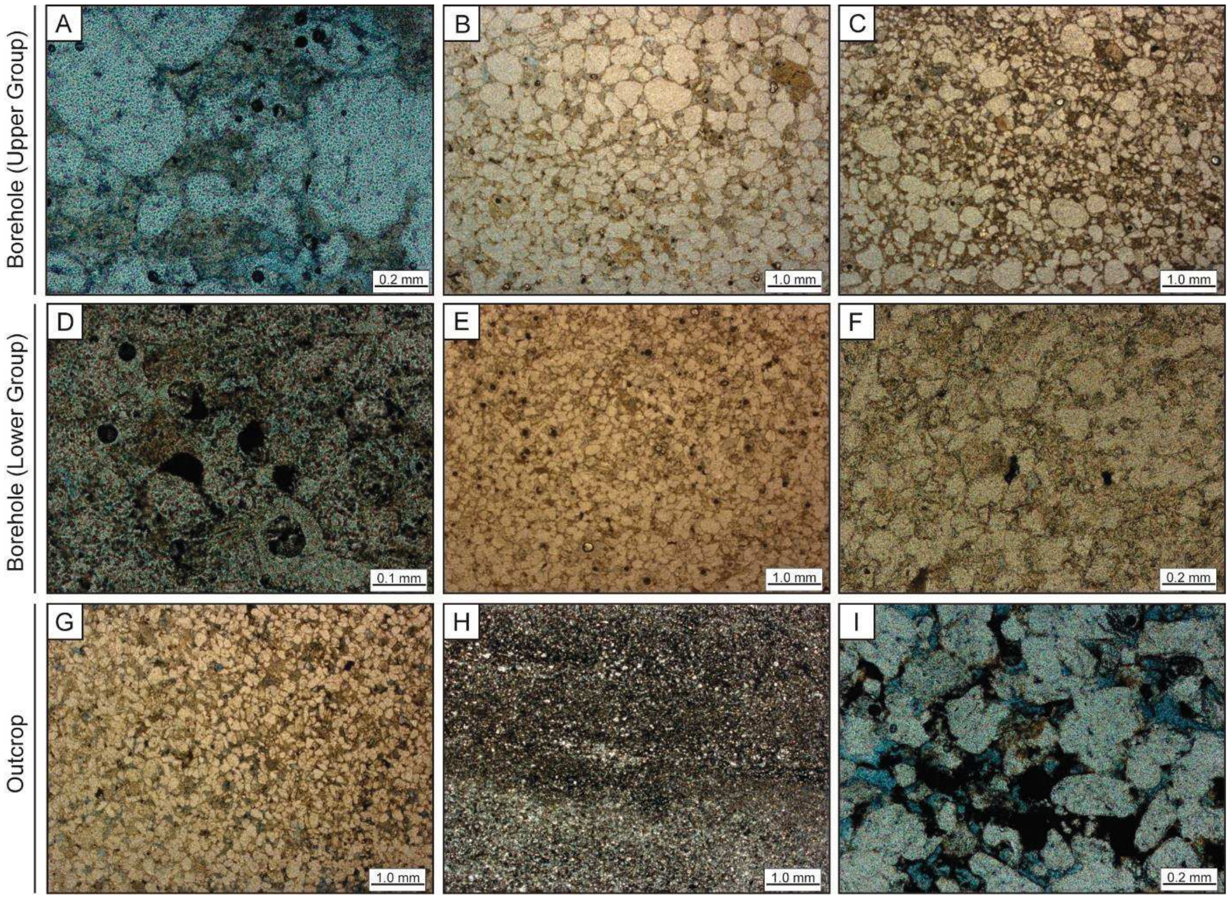

Figure 5. A) Dissolution features in sample CX27 in natural light (NL) (x10). B) Pore space filling by carbonate cement in sample CX33 in NL (x2.5). C) Bimodal grain size distribution in sample CX36 in NL (x2.5). D) Pyrite crystals inside pores in sample CX40 in NL (x20). E) Small grain size in sample CX44 in NL (x2.5). F) Tightly packed texture with little pore space in sample CX46 in NL (x10). G) Pyrite crystals (black spots) in pore space of sample PA02B in NL (x2.5). H) Siltstone with bioturbation structures in sample PA03A in NL (x2.5). I) Black to red ferruginous cement (hematite and goethite) in sample PA09A in LN (x10).

Sample PA02B from Corda Formation shows distinct petrographic characteristics compared to CXs samples. Grains are sub-rounded and well sorted. PA02B has higher porosity and cement in pore space compared to other sandstones. Cementation is similar to the lower group from Poti samples with initial illitic clay formation and occurrence of pyrite crystals (Fig. 5G). A sample from Pastos Bons Formation (PA03A) is a siltstone composed of quartz and mica. The sample shows a reddish ferruginous cementation (hematite and goethite). The principal feature in this sample are the bioturbation structures along with pyrite (Fig. 5H).

The Cabeças Formation sample (PA09A) shows a moderately sorted sand-sized framework composed mostly of mono- and polycrystalline quartz (>95%). Grains of plagioclase and K-feldspar occur, and rock fragments are rare. The sample has medium point to long compaction grain contacts. The porosity percentage is higher than the other samples and cementation is made of ferruginous minerals (hematite/goethite) and kaolinite (Fig. 5I).

4.2. Thermochronology

AFT and ZFT results are presented in Table 4. ZFT age distribution is shown in Figure 6. Thermal history models are presented in Figures 7 and 8.

4.2.1 Apatite Fission Track data

AFT data from borehole and outcrop samples have central ages expanding from 20.4 ± 7.8 to 130 ± 31 Ma. Samples CX33 and CX40 failed the χ^2-test indicating more than one age population. Apatite grains from sedimentary rocks show high partial annealing resetting with little or even no spontaneous fission tracks. Nonetheless, induced fission tracks in all apatite samples support AFT central age much younger than ZFT central ages of correlating samples (Table 4).

Among borehole samples, CX33 shows two age distributions with a higher proportion of a younger age of 16.8 ± 6.1 Ma (92%) compared to the older, 186 ± 41 Ma (8%). Sample CX40 shows similar two-age distribution of 7.7 ± 8 Ma (82%) and 140 ± 79 Ma (18%). In a lower position, CX44 recorded an average central age of 67 ± 8.7 Ma. In outcrop samples, PA02B shows a central age of 34 ± 8.6 Ma and MTL 8.92 ± 1.01 μm, and sample PA03A recorded an average central age of 130 ± 31 Ma and MTL 9.28 ± 0.79 µm. For these samples, measured Dpar values vary from 2.36 µm for PA03A to 1.28 µm for PA02B.

Table 4. Apatite and zircon fission track data

Sample	Dating Method	N	ρs (x10[5])	Ns	ρi (x10[5])	Ni	ρd (x10[5])	Nd	Central Age (Ma)	±1σ (Ma)	χ^2 (%)	U (ppm)	Dpar (µm)	n	MTL (µm)	S.D. (µm)	Group I Age (Ma) (%)	Group II Age (Ma) (%)
Borehole BPP																		
CX27	ZFT	39	73.3	3901	8.7	466	1.6	2500	92.8	9.3	0	194.7	-	-	-	-	57 (45)	172 (55)
CX33	AFT	22	0.5	67	1.0	125	19.7	6001	24.2	8.9	0	2.0	-	-	-	-	16 (92)	186 (8)
	ZFT	39	116.1	5695	5.2	253	1.6	2500	210.0	25.0	0	114.7	-	-	-	-	80 (16)	298 (84)
CX36	ZFT	49	97.1	4777	5.3	259	1.6	2500	182.0	23.0	0	117.1	-	-	-	-	92 (26)	291 (74)
CX40	AFT	31	0.2	22	0.7	90	19.7	6001	20.4	7.8	3	1.3	-	-	-	-	7 (82)	140 (18)
	ZFT	51	157.9	4909	3.0	92	1.6	2500	563.0	59.0	100	65.8	-	-	-	-	-	-
CX44	AFT	51	0.3	90	0.5	177	19.7	6001	67.0	8.7	78	1.0	-	-	-	-	-	-
	ZFT	31	134.0	3941	2.4	71	1.6	2500	576.0	76.0	36	53.7	-	-	-	-	-	-
CX46	ZFT	49	108.9	5244	3.6	172	1.6	2500	324.0	27.0	19	79.5	-	-	-	-	-	-
Outcrop																		
PA02B	AFT	50	0.1	28	0.3	91	19.7	6001	34.0	8.6	84	0.6	1.3	5	10.3	2.1	-	-
	ZFT	46	54.1	3229	8.2	487	1.6	2500	72.6	4.1	9	181.4	-	-	-	-	-	-
PA03A	AFT	18	1.7	92	1.2	64	19.7	6001	130.0	31.0	7	2.2	2.4	19	11.3	1.6	-	-
	ZFT	03	80.3	257	4.1	13	1.6	2500	215.0	61.0	36	90.4	-	-	-	-	-	-
PA06	ZFT	16	125.5	1310	2.7	28	1.6	2500	497.0	95.0	58	59.7	-	-	-	-	-	-
PA09A	ZFT	40	124.8	4963	3.0	118	1.6	2500	447.0	43.0	23	66.0	-	-	-	-	-	-

N: number of grains analyzed to determine track densities; ρs: measured spontaneous track density; Ns: number of spontaneous tracks counted; ρi: measured induced track density; Ni: number of induced tracks counted; ρd: track density measured in glass dosimeter; Nd: number of tracks counted in determining ρd; 1σ: standard deviation; χ2: Chi-square probability; U: calculated uranium content; Dpar: mean etch pit diameter of all measured etch pits; n: number of confined tracks lengths measured; MTL: mean track length; S. D.: standard deviation of track length distribution of individual track measurements; (-): not analysed. Note: AFT age calculated using C. Engelmann de Oliveira zeta-calibration, ζ-CN2 - 135.4.

4.2.2 Zircon Fission Track data

ZFT central ages expand from 72.6 to 576.0 Ma (Table 4 and Fig. 6). Zircon grains have U-concentration of 53.7–194.7 ppm (Table 4). Three samples failed the χ^2-test indicating more than one age population in the ZFT analyses. The uppermost sample CX27 shows two ages, one at 57.3 ± 4.2 Ma (45%) and an older at 172 ± 17 Ma (55%). Almost 29 m (95 ft) downward in the core, sample CX33 also shows two ages (80 ± 15 Ma and 298 ± 27 Ma), but with more grains from the oldest population (16% and 84%). Sample CX36 is located 10 m (32.8 ft) below CX33 and presents two ages, one at 92 ± 15 Ma (26%) and an older at 291 ± 34 Ma (74%). Stratigraphically below the three upper samples, CX40 shows a central age of 563 ± 59 Ma and CX44 an age of 576 ± 76 Ma. Both samples lack single grain ages younger than 185 Ma. The lowermost sample CX46 records a central age of 324 ± 27 Ma with a few single grain ages as low as 112 Ma.

Central age distributions in outcrop samples vary similar to the borehole. Sample PA02B shows a young central age of 72.6 ± 4.1 Ma, while Pastos Bons Formation sample (PA03A) records an older central age of 215 ± 61 Ma. Both samples are located close to an igneous intrusion (PA02A). Nevertheless, PA03A has fewer single grain ages which enhances the error. A Poti Formation sample (PA06) shows a central age of 497 ± 95 Ma and the Cabeças Formation sample (PA09A) an age of 447 ± 43 Ma.

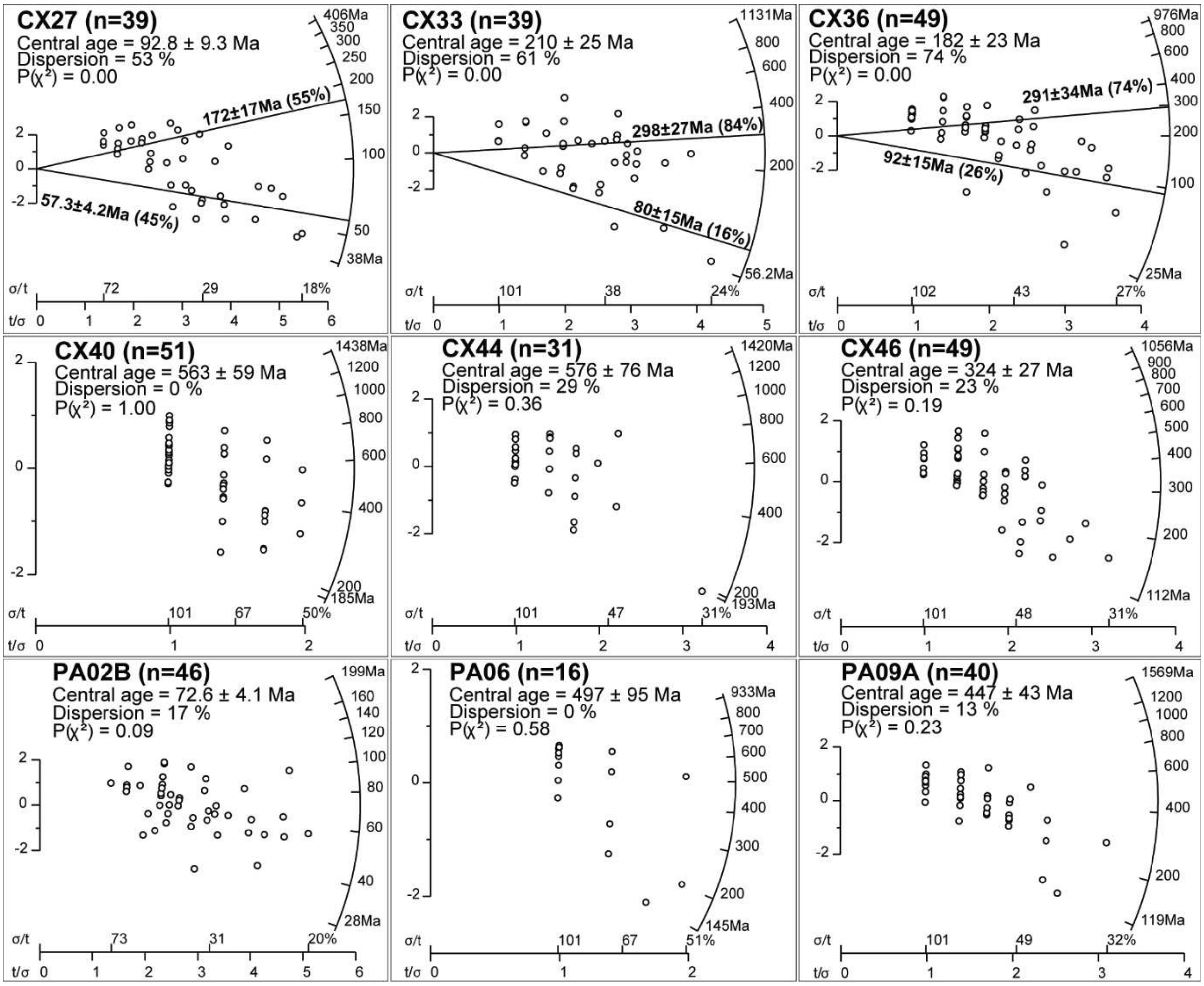

Figure 6. RadialPlotter diagrams of ZFT ages samples showing number of grains (n), central ages, dispersion and χ^2-test result.

4.2.3 Thermal history models

Based on fission-tracks parameters and geological background of the area, inversion models for the samples were conducted using the pre-defined constraints (Fig. 7). The best-fit thermal models from borehole samples show maximum post-depositional paleotemperatures decreasing with depth and all occurring from ca. 102 to 201 Ma. Sample CX27 shows good fitting paths with an initial constant heating reaching beyond the apatite partial annealing zone (PAZ) with a maximum paleotemperature of ca. 367 °C (692.6 °F) at 102 Ma, then a rapid cooling to present-day temperature. Likewise, samples CX33 and CX36 show increasing paleotemperatures until 130 and 136 Ma, when reached a maximum paleotemperature of 308 °C (586.4 °F) and 313 °C (595.4 °F), respectively, followed by a final cooling event to present-day temperature.

Borehole samples CX40 and CX44 show a pre-depositional thermal history which recorded a maximum paleotemperature of ca. 600 to 560 Ma. After deposition, the rocks experienced a heating phase, in which the samples reached a maximum paleotemperature of ca. 149 °C (300.2 °F) and 143 °C (289.4 °F) at 133 and 155 Ma, respectively. Good fitting paths of sample CX46 record heating to a maximum temperature of ca. 123 °C (253.4 °F) at 201 Ma, followed by a cooling event to present-day temperature.

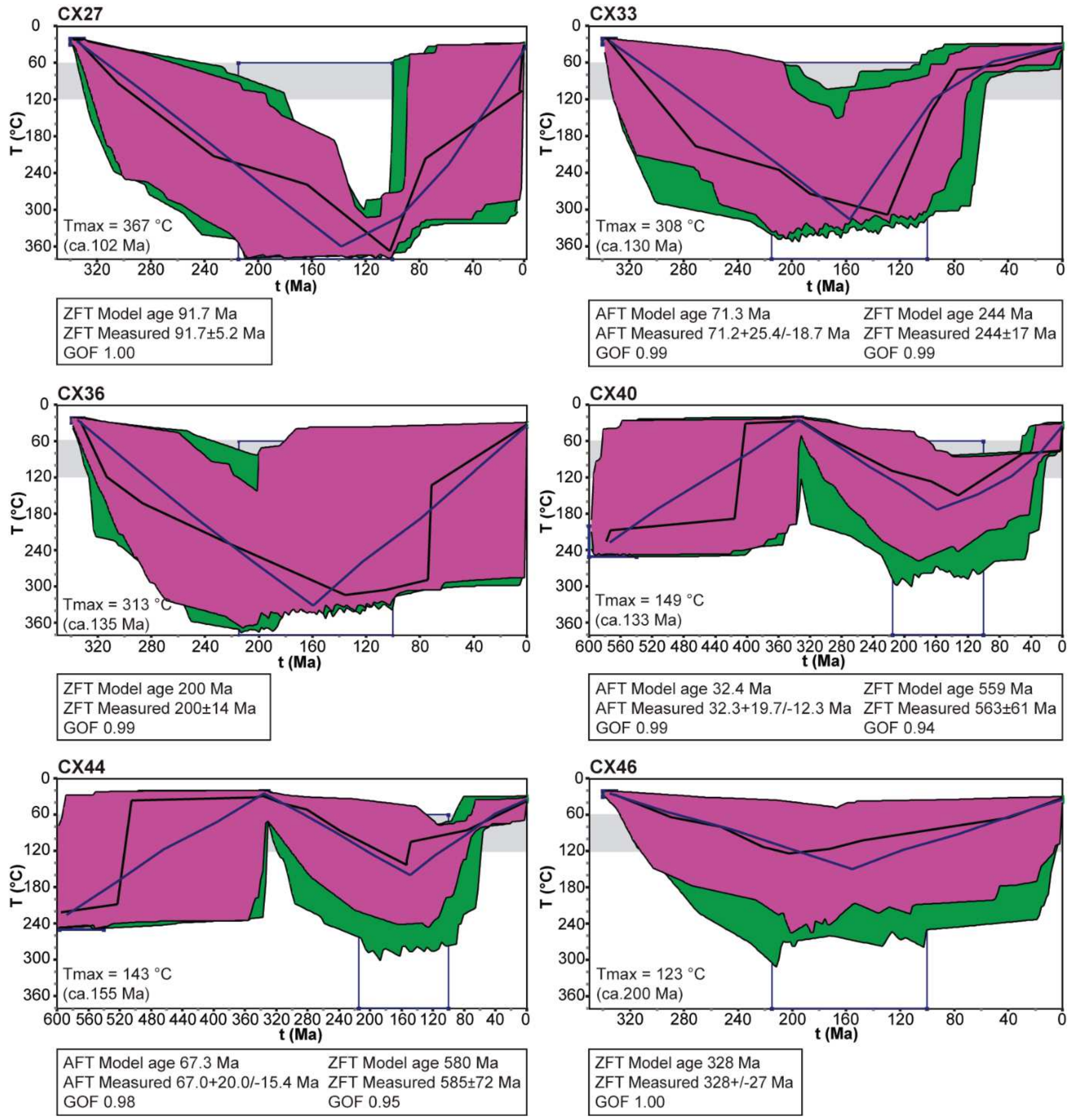

Figure 7. Thermal histories models from HeFTy software (Ketcham, 2005) for borehole samples (CXs). Green, purple and blue lines represent acceptable, good and weighted mean fitting t-T paths, respectively. Gray boxes indicate the apatite partial annealing zone. Blue boxes are t-T constraints.

Good fitting paths of sample PA03A show post-depositional heating to a maximum paleotemperature of ca. 72 °C (161.6 °F) at 108 Ma, and thereafter a cooling phase until present-day temperature. The best-fit thermal model from sample PA02B shows a sudden heating during deposition-time to a maximum paleotemperature of ca. 355 °C (671 °F) during 45 Myr, then a rapid cooling to PAZ temperature and thereafter to present-day temperature (Fig 8).

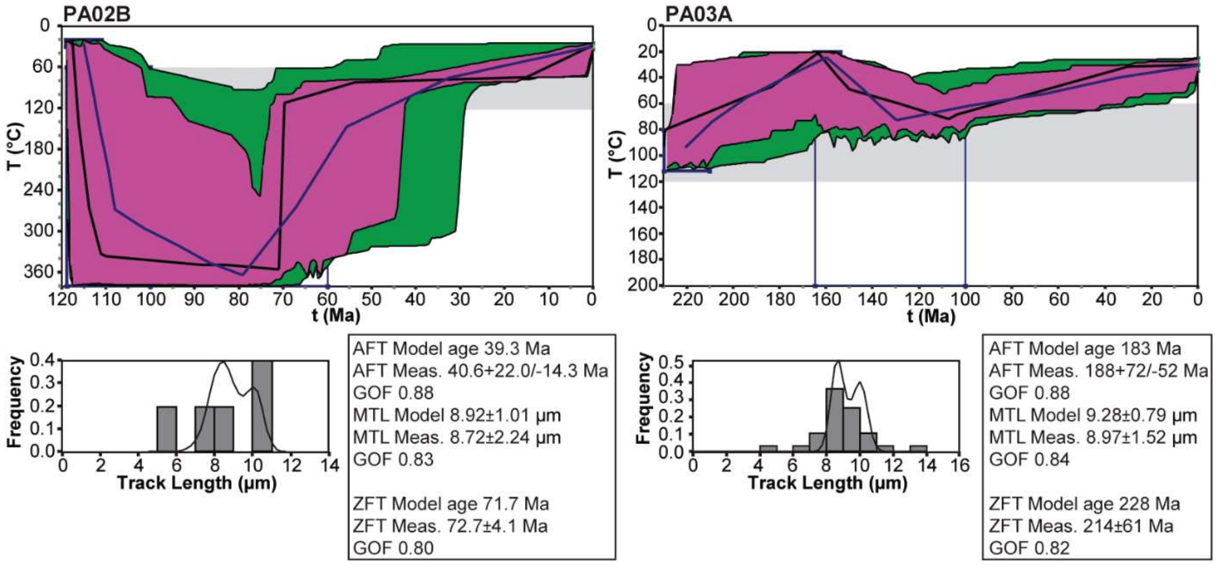

Figure 8. Thermal histories models from HeFTy software (Ketcham, 2005) for outcrop samples. Green, purple and blue lines represent acceptable, good and weighted mean fitting t-T paths, respectively. Gray boxes indicate the apatite partial annealing zone. Blue boxes are t-T constraints.

5 DISCUSSIONS

5.1. Dimension of the Thermal Effect of Potential Reservoir Rocks

Borehole samples are separated in two groups (upper and lower) by depositional and diagenetic properties, and the groups are also reflected in the thermochronology data which records a diverse thermal history. All AFT ages are much younger than depositional age and indicate a partial or total reset related to elevated temperature (above apatite PAZ) from the nearby igneous intrusion. Differently, ZFT central ages record pre- and post-depositional ages. Post-depositional ages indicate a thermal influence of the two magmatic events, although the last event (Sardinha Formation) is better evidenced in the samples that show a clear division between the two groups in terms of maximum paleotemperature.

Comparing petrographic characteristics, the upper group (CX27, CX33 and CX36) shows larger, low spherical and moderately sorted grains, implying less transport and reworking than the lower group (CX40, CX44 and CX46), which is composed of smaller and spherical grains. Besides, the lower group has mica sheets between quartz grains implying a low energy system compared to the upper group. Stages of eodiagenesis in all samples show precipitation of kaolinite inside pore spaces. Spaces are also filled with quartz cement (chalcedony) overgrowing quartz grains. Compaction grain contacts emphasize that the samples were compacted enough to rearrange the grains and diminish the primary porosity when mechanical compaction started. The presence of secondary porosity by grain dissolution is linked to the high temperature fluid percolation from the later intrusion of igneous rocks of Mosquito and Sardinha Formations. This porosity was then filled with quartz cement and kaolinite from quartz and feldspar dissolution. The dissolution of detrital K-feldspar grains implies in temperature ca. 50-150 °C (122-302 °F) (Wilkinson et al., 2001) and the replacement by authigenic clay minerals (kaolinite) occurs at ca. 50–150 °C (122-302 °F) (e.g. Verdel et al., 2012; Wilkinson et al., 2001). The correlation of porosity with average grain size shows that fewer pore spaces in the lower group probably result from major compaction of smaller grains. Differently, the upper group shows a higher porosity possibly due to the larger grains and the hydrothermal influence of the intrusion (Houseknecht, 1988).

In terms of thermochronology, the upper group is positioned below the igneous sill and shows a high magnitude influence from the intrusion demonstrated by increase in older ZFT ages with depth until sample CX36 (Fig. 6). These results of sample ages show a clear reduction in thermal effects with depth. Furthermore, in terms of maximum paleotemperature, inversion models of the upper group samples show influence up to sample CX36, in which samples underwent temperatures from ca. 367 °C (692.6 °F) in CX27 to 313 °C (595.4 °F) in CX36, correlated to the Sardinha Formation intrusion event (Fig. 9). These paleotemperatures are similar to Rodrigues (1995) using vitrinite reflectance in a different area of the basin. Although the intrusion affected all samples, the results also show a great decay in thermal influence between samples CX36 and CX40 (ca. 313 °C to 149 °C (595.4 °F to 300.2 °F)) which corresponds to a significant limit to the intrusion influence. Thereby, the high temperature influence (>225 °C (437 °F)) is verified until ~51 m (167.3 ft) from the intrusion contact with the sedimentary rocks (Fig. 9). This distance is comparable to the influence described by Rodrigues (1995) of 0.8 to 1.3 times the size of the igneous body. However, we are unable to make correlation with size because the intrusion is altered at the top of the section. The high temperature (above the apatite PAZ) experienced by all apatite samples from the borehole is verified by the high partial annealing of the spontaneous fission tracks.

The lower group (~60 m (196.8 ft) distant from the intrusion; Fig. 9) shows pre-depositional ZFT central ages varying from 560 to 600 Ma, correlated to the Brasiliano orogeny, the last major tectonic event of the pre-depositional history. Nonetheless, a few zircon grains (<10%) record ages younger than 200 Ma and indicate a thermal influence from the upper intrusion (Sardinha Formation), but also record the influence of the older intrusion in the basin, the Mosquito Formation (~200 Ma). Sample CX46 records a ZFT central age of 324 ± 27 Ma which correlates to the initial depositional age of the Poti Formation. Inversion models of the lower group show that maximum post-depositional temperatures vary from ca. 149 to 123 °C (300.2 to 253.4 °F) (Fig. 7). The lowermost sample (CX46) records the maximum paleotemperature related to the Mosquito Formation (~200 Ma), which is associated to the CAMP event that largely affected the Parnaíba Basin (Merle et al., 2011).

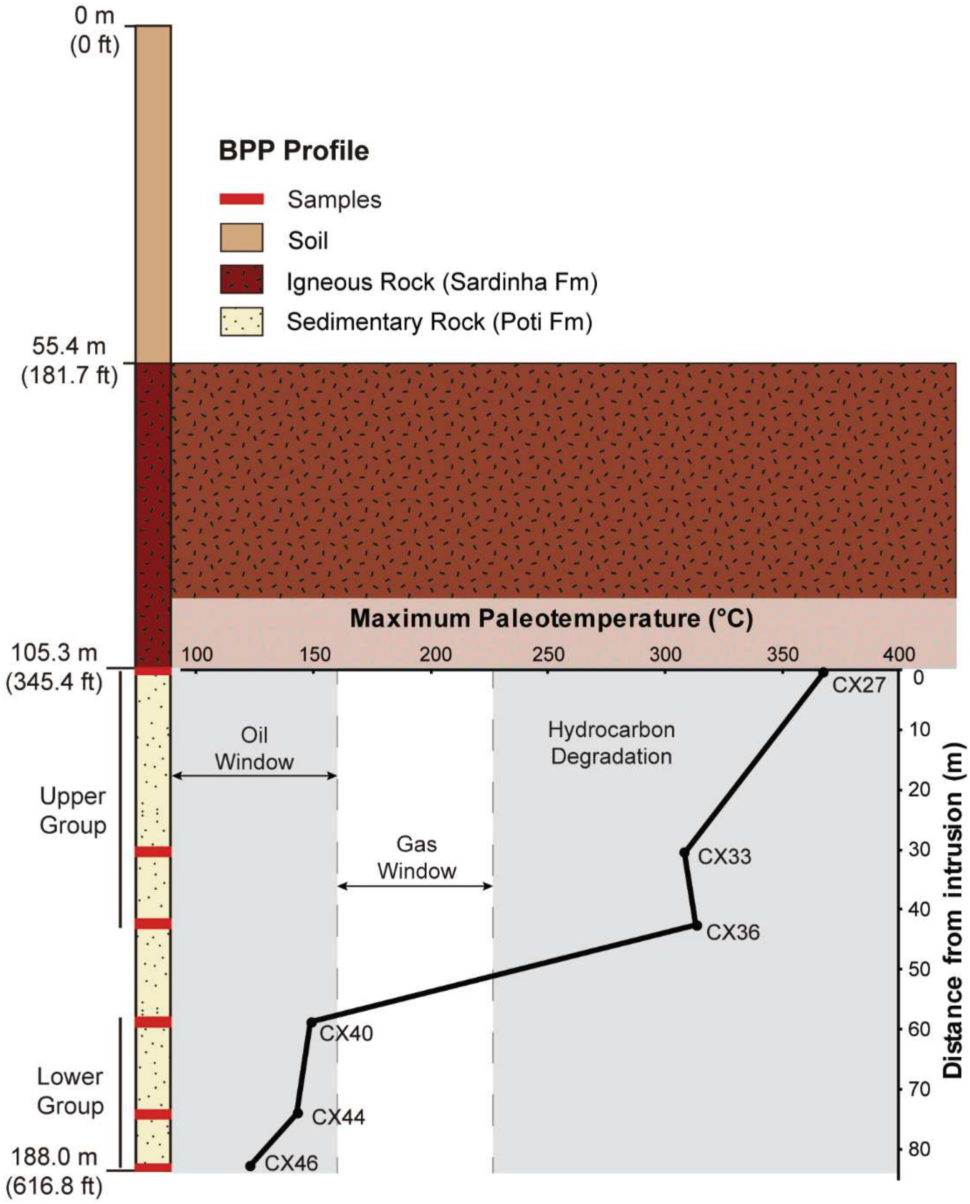

Figure 9. Maximum paleotemperature profile for borehole samples. Between samples CX36 and CX40, there is an important decay in the thermal influence from the upper igneous rocks. Below ca. 50 m (164 ft) from the intrusion, the sedimentary rocks maintained low temperatures and the reservoir layer stayed unmodified.

Regarding the petroleum system, the maximum paleotemperatures experienced by the upper group samples altered the physical properties of the reservoir rocks in the Parnaíba Basin. Moreover, paleotemperatures above 225 °C (437 °F) which were estimated for sandstone potential reservoir layers (Upper Group, Fig. 9) and intruded by later Sardinha Formation magmatism, modified significantly the fabric of these rocks. Reservoir layers which experience these high temperatures underwent hydrocarbon dehydration forming varying carbonic products (e.g. graphite) (Vandenbroucke et al., 1999). High temperatures also resulted in hydrothermal fluid percolation and alteration of framework grains (quartz and feldspars). High temperature fluids from the intrusion caused almost total feldspar dissolution, increasing the porosity in the upper group. However, after the thermal influence, fluids rich in carbonate and silica started to precipitate minerals in pore spaces, increasing substantially cementation, as shown in Table 3. Even with porosity enhancement caused by grain dissolution, the formation of carbonate cement is not favorable in a reservoir context because it decreases the permeability (Bjørlykke et al., 1989; Poelchau et al., 1997; Ahmed, 2002; Taylor et al., 2010).

In the lower group, we can observe a mixture of thermal influence in the maximum paleotemperatures. This is explained by an older high intensity thermal event related to the Mosquito Formation coming from lower depths of the basin, and a younger influence from the upper intrusion (Sardinha Formation) acting on this group. In terms of temperature, these samples are favorable for hydrocarbon reservoir, because they kept paleotemperature high enough to alter the reservoir layer (>225 °C (437 °F)). However, diagenetic aspects do not endorse the capability because compared to the upper group, the grain dissolution in the lower group created less secondary porosity and the mechanical compaction was probably enhanced by overburden from the igneous rocks. Porosity of samples shows compact sandstones with less than 10% porous space, unfavorable condition for reservoir rocks (Table 3). Also, early illitization and pyrite presence is described in samples from the lower group. According to Rickard (1997), authigenic pyrite forms in stable conditions from 25 to 125 °C (77 to 257 °F). The occurrence of euhedral pyrite in pore space in these rocks implies in early diagenesis of shallow marine deposits with low organic matter leading to low rates of sulfide production. The process is different from mud-rich rocks with higher contents of sulphur which results in framboidal pyrites, after microbial organisms supersaturate the intraporous fluids (Taylor and Macquaker, 2000). In this case, sand-rich rocks of the lower group have low FeS saturation precipitating small nearly euhedral intrapore pyrite. The absence of pyrite crystals in the upper group suggests a deficiency in organic matter during early diagenesis or even destabilization of FeS by high paleotemperature fluids in these rocks.

5.2. Thermal History and Petroleum Systems of the Eastern Margin

In the eastern edge of the Parnaíba Basin, the thermochronological results reveal that all samples were thermally influenced by the two magmatic events, Mosquito (~200 Ma) and Sardinha (120-130 Ma), however the last event is better registered. We analyzed two sets of samples; those from the BPP borehole record the decay of thermal influence near an intrusive rock, and the outcrop samples show the regional thermal influence of the magmatic events.

Borehole samples of the Poti Formation evidence the thermal influence allowing an estimative of thermal decay in the borehole (Fig. 9). In a separate set of samples, outcrop sample PA06, collected far from an intrusion, records a pre-depositional ZFT central age. However, the youngest ZFT age of ~145 Ma if from a zircon grain completely reset by intrusions of the Sardinha Formation. This sample points to the regional thermal influence of the last event in this part of the basin.

The Cabeças Formation outcrop sample PA09A records a ZFT central age of provenance, nevertheless it also records zircon grain ages associated in time to the younger magmatic intrusion (Sardinha Formation) at ~120 Ma. Petrographic information of this sample shows moderate sorting and more angular and irregular grain shapes, implying shorter grain transport. Grain contacts in this sample have medium point to length compaction and higher porosity than Poti samples (Table 3). The rock is cemented by opaque ferruginous minerals indicating a transitional to continental environment with meteoric water percolation and oxidation.

Sample PA03A from the Pastos Bons Formation is from a typically low energy environment with fine quartz and mica grains. The rock is cemented by opaque minerals of black-reddish color indicating ferruginous minerals. The sample shows bioturbation marks indicating paralic environment with biotic action along with nearly euhedral pyrite minerals, an indication of reductive context (Worden and Morad, 2003). Euhedral pyrite also indicates low saturation in sulphate (Taylor and Macquaker, 2000). Thermochronological data for this sample show AFT central age of 130 ± 31 Ma indicating a major influence from the Sardinha Formation and a maximum paleotemperature of ca. 71°C (159.8 °F) related to this intrusion (Fig. 8).

Stratigraphically above of Sardinha Formation, sample PA02B from Corda Formation has fine sand of low sphericity, composed of angular grains and larger pore spaces than Poti Formation samples. Cementation is by carbonate minerals with early illitization of micaceous minerals and presence of euhedral, intrapore pyrite. Inversion model of the AFT and ZFT data shows heating event coeval to deposition (Fig. 8). This is not well resolved but represents Corda Formation sandstone deposition associated to an intrusive event of the Sardinha Formation, which explains the correlated deposition and thermal influence of this sample.

In the context of the Parnaíba Basin, the Mosquito and Sardinha Formations strongly affected the sedimentary rocks and surrounding basement rocks. The first event (Mosquito Formation) is associated in time to the large igneous province CAMP (Marzoli et al., 2018; Svensen et al., 2018) that affected the western part of Gondwana during the early stage of paleocontinent break-up. Regionally, in the western basement rocks of the basin, Dias et al. (2017) used Fission Track dating of zircon grains from Archean to Paleoproterozoic granites and gneisses and determined younger fission track ages of ~200 Ma reflecting crustal heating associated with the Lower Jurassic Mosquito. These authors attributed a significant role to this event in the production of heat for hydrocarbon generation in the Parnaíba basin. Also, Klein et al. (2013) dated intrusions in the São Luís craton in the northwestern edge of the basin, correlated in time to the Mosquito event. These studies show the large extension of CAMP overlying the basement rocks and the Paleozoic Basin. In the sedimentary rocks of the Parnaíba Basin, CAMP is linked to the western edge of the basin in which intrusive bodies of the Mosquito Formation are exposed (De Min et al., 2003; Merle et al., 2011; Mocitaiba et al., 2017).

Sardinha Formation is described in the eastern edge of the basin (Oliveira et al., 2018) and linked to another large igneous province, the Paraná-Etendeka Magmatism, which is a later phase of Gondwana break-up in the southern Atlantic Ocean margin (Mizusaki et al., 2002). The event is connected to diverse intrusive rocks in eastern Brazil, including the Rio Ceará–Mirim Dike Swarm (de Castro et al., 2018) in the eastern basement rocks of the Parnaíba Basin.

The samples analyzed in this study reveal thermal influence of both magmatic events in the eastern edge of the basin. AFT central ages are correlated with the last event, while ZFT ages record pre-depositional ages correlated to the Brasiliano orogeny, although a few single grains evidence the thermal influence of Mesozoic magmatic events. Associating the results to petroleum systems, the older Mosquito event thermally influenced the generation of hydrocarbon as described by Rodrigues (1995) and Porto and Pereira (2014). In the studied area, the late Sardinha event also acted in hydrocarbon generation, although the intrusion event altered the reservoir rocks by intruding in reservoir layers and enhancing the maximum paleotemperatures as shown in the borehole samples. In this way, the disposition of laccolith bodies of the Sardinha Formation altered the reservoir layers in this part of the Parnaíba Basin.

6 CONCLUSIONS

In this study, all samples had minor hydrocarbon abundance but help identify thermal effects of surrounding igneous rocks in potential reservoir rocks. The AFT, ZFT and petrographic data allow us to identify that the intrusions acted as thermal enhancement to hydrocarbon, but on the other hand, the intrusion altered the reservoir layer in the eastern part of the Parnaíba Basin. Results also validate an innovative approach for thermochronological studies in delimiting thermal histories of petroleum systems. The main conclusions of this study are:

(1) Thermochronological data show influences from two magmatic events, but the major influence in the eastern part of the Parnaíba Basin is related to the last Sardinha Formation.

(2) The intrusion effects in Poti and Cabeças samples increased the dissolution, carbonate precipitation and compaction in the rocks due to higher temperature fluid percolation and overburden in the system.

(3) Pastos Bons Formation sample was thermally influenced by the intrusion. However, the rocks show no diagenetic features or porosity for a potential reservoir. The deposition history of the Corda Formation sample is close in time with the Sardinha intrusion, thus duration of intrusion was short to constrain a potential reservoir context.

(4) In borehole samples closer than ca. 50 m (164 ft) to magmatic activity, the reservoir properties were obliterated by high temperature (>225 °C (437 °F)) and secondary diagenetic effects.

(5) In the lower group of borehole samples, farther than ca. 50 m (164 ft) from the intrusion, the maximum paleotemperatures were sufficiently low so potential

reservoir layers remained unaltered, but compaction was enhanced by igneous overburden.

Acknowledgements

The authors acknowledge Project POTI ANP-UnB-PGN for financial and scientific support and Andrew Carter for dosimeter glasses. We are also thankful to the professor Léo A. Hartmann for reviewing this manuscript. The first author thanks CAPES (Coordenação de Aperfeiçoamento de Pessoal de Nível Superior) within the Ministry of Education of Brazil for the student grant (PROSUC/88887.150578/2017-00).

REFERENCES CITED

Ahmed, W., 2002, Effects of heat-flow and hydrothermal fluids from volcanic intrusions on authigenic mineralization in sandstone formations: Bulletin of the Chemical Society of Ethiopia, v. 16, no. 1, p. 37-52, doi: 10.4314/bcse.v16i1.20947

Allen, P. A., and J. R. Allen, 2013, Basin analysis: Principles and application to petroleum play assessment: Oxford, UK, John Wiley & Sons, 632 p.

Almeida, F. F. M., and C. D. R. Carneiro, 2004, Inundações marinhas fanerozóicas no Brasil e recursos minerais associados, *in* V. Mantesso-Neto, A. Bartorelli, C. D. R. Carneiro, and B. B. Brito-Neves, eds., Geologia do continente sul-americano: evolução da obra de Fernando Flávio Marques de Almeida: São Paulo, Beca, p. 43-58.

ANP, 2015, Bacia do Parnaíba: Sumário Geológico e Setores em Oferta – 13ª Rodada de Licitações, accessed October 15, 2017, http://www.anp.gov.br/.

ANP, 2017, Boletim da Produção de Petróleo e Gás Natural – Circulação Externa. Setembro 2017/ Número 85, accessed October 18, 2017, http://www.anp.gov.br/.

Araújo, R. N., A. C. R. Nogueira, J. Bandeira, and R. S. Angélica, 2016, Shallow lacustrine system of the Permian Pedra de Fogo Formation, Western Gondwana, Parnaíba Basin, Brazil: Journal of South American Earth Sciences, v. 67, p. 57-70, doi: 10.1016/j.jsames.2016.01.009

Baksi, A. K., and D. A. Archibald, 1997, Mesozoic igneous activity in the Maranhão province, northern Brazil: 40Ar/39Ar evidence for separate episodes of basaltic magmatism: Earth and Planetary Science Letters, v. 151, no. 3-4, p. 139-153, doi: 10.1016/S0012-821X(97)81844-4

Becker, R. T., 1993, Anoxia, eustatic changes, and Upper Devonian to lowermost Carboniferous global ammonoid diversity, *in* M. R. House, ed., The Ammonoidea: environment, ecology, and evolutionary change: Oxford University Press, p. 115-164

Bernet, M., and J. I. Garver, 2005, Fission-track analysis of detrital zircon: Reviews in Mineralogy and Geochemistry, v. 58, no. 1, p. 205-237, doi: 10.2138/rmg.2005.58.8

Bjørlykke, K., M. Ramm, and G. C. Saigal, 1989, Sandstone diagenesis and porosity modification during basin evolution: Geologische Rundschau, v. 78, no. 1, p. 243-268, doi: 10.1007/BF01988363

Brito Neves, B. B., 2002, Main stages of the development of the sedimentary basins of South America and their relationship with the tectonics of supercontinents: Gondwana Research, vol. 5, no. 1, p. 175–196. doi: 10.1016/S1342-937X(05)70901-1

Brown, R., K. Gallagher, and M. Duane, 1994, A quantitative assessment of the effects of magmatism on the thermal history of the Karoo sedimentary sequence: Journal of African Earth Sciences, v. 18, no. 3, p. 227-243, doi: 10.1016/0899-5362(94)90007-8

Burke, K., D. S. MacGregor, and N. R. Cameron, 2003, Africa's petroleum systems: four tectonic 'Aces' in the past 600 million years: Geological Society, London, Special Publications, v. 207, no. 1, p. 21-60, doi: 10.1144/GSL.SP.2003.207.3

Cunha, P. R., A. R. Bianchini, J. L. Caldeira, and C. C. Martins, 2012, Parnaíba Basin - The Awakening of a Giant: XI Simposio Bolivariano Exploración Petrolera en las Cuencas Subandinas, Cartagena, Colombia, July 29-August 1, 2012.

Daly, M. C., V. Andrade, C. A. Barousse, R. Costa, K. McDowell, N. Piggott, and A. J. Poole, 2014, Brasiliano crustal structure and the tectonic setting of the Parnaíba basin of NE Brazil: Results of a deep seismic reflection profile: Tectonics, v. 33, no. 11, p. 2102-2120, doi: 10.1002/2014TC003632

de Castro, D. L., D. C. Oliveira, and M. H. B. Hollanda, 2018, Geostatistical Interplay Between Geophysical and Geochemical Data: Mapping Litho-Structural Assemblages of Mesozoic Igneous Activities in the Parnaíba Basin (NE Brazil): Surveys in Geophysics, p. 1-31, doi: 10.1007/s10712-018-9463-5

de Castro, D. L., F. H. R. Bezerra, R. A. Fuck, and R. M. Vidotti, 2016, Geophysical evidence of pre-sag rifting and post-rifting fault reactivation in the Parnaíba basin, Brazil: Solid Earth, v. 7, p. 529-548, doi: https://doi.org/10.5194/se-7-529-2016

de Castro, D. L., R. A. Fuck, J. D. Phillips, R. M. Vidotti, F. H. Bezerra, and E. L. Dantas, 2014, Crustal structure beneath the Paleozoic Parnaíba Basin revealed by airborne gravity and magnetic data, Brazil: Tectonophysics, v. 614, no. 18, p. 128-145, doi: 10.1016/j.tecto.2013.12.009

De Min A., E. M. Piccirillo, A. Marzoli, G. Bellieni, P. R. Renne, M. Ernesto and L. S. Marques, 2003, The Central Atlantic Magmatic Province (CAMP) in Brazil: petrology, geochemistry, $^{40}Ar/^{39}Ar$ ages, paleomagnetism and geodynamic implications. The central Atlantic magmatic province: insights from fragments of Pangea, *in* W. Hames, J. G. McHone, P. C. Renne, and C. Ruppel, eds., The Central Atlantic Magmatic Province: Insights from Fragments of Pangea: Geophysical Monograph Series, v. 136, p. 91-128, doi: 10.1029/136GM06

Della Fávera, J. C., 1990, Tempestitos da Bacia do Parnaíba, Doctoral's thesis, Instituto de Geociências/Universidade Federal do Rio Grande do Sul, Porto Alegre, RS, 243 p.

Dias, A. N. C., C. A. V. Moura, J. M. Neto, F. Chemale Jr, T. J. Girelli, and K. M. Masuyama, 2017, Geochronology and thermochronology of the gneisses of the Brasiliano/Pan-African Araguaia Belt: Records of exhumation of West Gondwana and Pangea break up: Journal of South American Earth Sciences, v. 80, p. 174-191, doi: 10.1016/j.jsames.2017.09.027

Dickinson, W. R., L. S. Beard, G. R. Brakenridge, J. L. Erjavec, R. C. Ferguson, K. F. Inman, R. A. Knepp, F. A. Lindberg, and P. T. Ryberg, 1983, Provenance of North America Phanerozoic sandstones in relation to tectonic setting: Geological Society of America Bulletin, v. 94, no. 2, p. 222-235, doi: 10.1130/0016-7606(1983)94<222:PONAPS>2.0.CO;2

Donelick, R. A., P. B. O'Sullivan, and R. A. Ketcham, 2005, Apatite fission-track analysis: Reviews in Mineralogy and Geochemistry, v. 58, no. 1, p. 49-94, doi: 10.2138/rmg.2005.58.3

Dumitru, T. A., 1993, A new computer-automated microscope stage system for fission-track analysis: Nuclear Tracks and Radiation Measurements, v. 21, no. 4, p. 575-580, doi: 10.1016/1359-0189(93)90198-I

Engelmann de Oliveira, C. H., A. R. Jelinek, F. Chemale Jr, and J. A. Cupertino, 2016, Thermotectonic history of the southeastern Brazilian margin: Evidence from apatite fission track data of the offshore Santos Basin and continental basement: Tectonophysics, v. 685, no. 20, p. 21-34, doi: 10.1016/j.tecto.2016.07.012

Fodor, R. V., A. N. Sial, S. B. Mukasa, and E. H. McKee, 1990, Petrology, isotope characteristics, and K-Ar ages of the Maranhao, northern Brazil, Mesozoic basalt province: Contributions to Mineralogy and Petrology, v. 104, no. 5, p. 555-567, doi: 10.1007/BF00306664

Galbraith, R. F., and G. M. Laslett, 1993, Statistical models for mixed fission track ages: Nuclear tracks and radiation measurements, v. 21, no. 4, p. 459-470, doi: 10.1016/1359-0189(93)90185-C

Góes, A. M. O., 1995, Formação Poti (Carbonífero inferior) da Bacia do Parnaíba, Doctoral's thesis, Universidade de São Paulo, São Paulo, SP, 204 p.

Góes, A. M. O., and F. J. Feijó, 1994, Bacia do Parnaíba: Boletim de Geociências da PETROBRAS, v. 8, no. 1, p. 57-67.

Góes, A. M. O., J. M. P. Souza, and U. B. Teixeira, 1990, Estágio Exploratório e Perspectivas Petrolíferas da Bacia do Parnaíba: Boletim de Geociências da PETROBRAS, v. 4, no. 1, p. 55–64.

Green, P. F., 1981, A new look at statistics in fission-track dating: Nuclear tracks, v. 5, no. 1-2, p. 77-86, doi: 10.1016/0191-278X(81)90029-9

Green, P. F., P.V. Crowhurst, and I. R. Duddy, 2004, Integration of AFTA and (U-Th)/He thermochronology to enhance the resolution and precision of thermal history reconstruction in the Anglesea-1 well, Otway Basin, SE Australia: Eastern Australasian Basins Symposium (EABS), Adelaide, Australia, September 19-22, 2004.

Houseknecht, D. W., 1988, Intergranular pressure solution in four quartzose sandstones: Journal of Sedimentary Research, v. 58, no. 2, p. 228-246, doi: 10.1306/212F8D64-2B24-11D7-8648000102C1865D

Hurford, A. J., 1990, Standardization of fission track dating calibration: Recommendation by the Fission Track Working Group of the IUGS Subcommission on Geochronology: Chemical Geology: Isotope Geoscience Section, v. 80, no. 2, p. 171-178, doi: 10.1016/0168-9622(90)90025-8

Hurford, A. J., and P. F. Green, 1983, The zeta age calibration of fission-track dating: Chemical Geology, v. 41, p. 285-317, doi: 10.1016/S0009-2541(83)80026-6

Ketcham, R. A., 2005, Forward and inverse modeling of low-temperature thermochronometry data: Reviews in mineralogy and geochemistry, v. 58, no. 1, p. 275-314, doi: 10.2138/rmg.2005.58.11

Ketcham, R. A., A. Carter, R. A. Donelick, J. Barbarand, and A. J. Hurford, 2007, Improved modeling of fission-track annealing in apatite: American Mineralogist, v. 92, no. 5-6, p. 799-810, doi: 10.2138/am.2007.2281

Kingston, J., and J. R. Matzko, 1995, Undiscovered petroleum of the Brazilian interior sag basins: International Geology Review, v. 37, no. 11, p. 959-980, doi: 10.1080/00206819509465435

Klein, E. L., R. S. Angélica, C. Harris, F. Jourdan, and M. Babinski, 2013, Mafic dykes intrusive into Pre-Cambrian rocks of the São Luís cratonic fragment and Gurupi Belt (Parnaíba Province), north–northeastern Brazil: Geochemistry, Sr–Nd–Pb–O isotopes, 40Ar/39Ar geochronology, and relationships to CAMP magmatism: Lithos, v. 172, p. 222-242, doi: 10.1016/j.lithos.2013.04.015

Linol, B., M. J. de Wit, C. H. Kasanzu, R. da Silva Schmitt, F. J. Corrêa-Martins, and A. Assis, 2016, Correlation and paleogeographic reconstruction of the Cape-Karoo basin sequences and their equivalents across central west Gondwana, *in* B. Linol, and M. de Wit, eds., Origin and Evolution of the Cape Mountains and Karoo Basin: Regional Geology Reviews, p. 183-192, doi: 10.1007/978-3-319-40859-0_18

Magoon, L. B., and W. G. Dow, 1994, The petroleum system: From source to trap: Tulsa, AAPG Memoir 60, 655 p.

Marzoli, A., P. R. Renne, E. M. Piccirillo, M. Ernesto, G. Bellieni, and A. De Min, 1999, Extensive 200-million-year-old continental flood basalts of the Central Atlantic

Magmatic Province: Science, v. 284, no. 5414, p. 616-618, doi: 10.1126/science.284.5414.616

Marzoli, A., S. Callegaro, J. Dal Corso, J. H. Davies, M. Chiaradia, N. Youbi, H. Bertrand, L. Reisberg, R. Merle, and F. Jourdan, 2018, The Central Atlantic Magmatic Province (CAMP): A Review, *in* L. Tanner, ed., The Late Triassic World: Topics in Geobiology, v. 46, p. 91-125, doi: 10.1007/978-3-319-68009-5_4

Merle, R., A. Marzoli, H. Bertrand, L. Reisberg, C. Verati, C. Zimmermann, M. Chiaradia, G. Bellieni, M. Ernesto, 2011, $^{40}Ar/^{39}Ar$ ages and Sr–Nd–Pb–Os geochemistry of CAMP tholeiites from Western Maranhão basin (NE Brazil): Lithos, v. 122, no. 3, p. 137-151, doi: 10.1016/j.lithos.2010.12.010

Milani, E. J., and P. V. Zalán, 1999, An outline of the geology and petroleum systems of the Paleozoic interior basins of South America: Episodes, v. 22, p. 199-205.

Miranda, F., P. R. Cunha, J. Caldeira, F. Aragão, and D. Michelon, 2016, The atypical igneous-sedimentary petroleum systems of the Parnaíba basin: Seismic, well-logs and analogues: International Conference and Exhibition, Barcelona, Spain, April 3-6, 2016, p. 220-220, doi: 10.1190/ice2016-6471370.1

Mizusaki, A. M. P., A. Thomaz Filho, E. J. Milani, and P. De Césero, 2002, Mesozoic and Cenozoic igneous activity and its tectonic control in northeastern Brazil: Journal of South American Earth Sciences, v. 15, no. 2, p. 183-198, doi: 10.1016/S0895-9811(02)00014-7

Mocitaiba, L. S. R., D. L. de Castro, and D. C. de Oliveira, 2017, Cartografia geofísica regional do magmatismo mesozoico na Bacia do Parnaíba: Geologia USP. Série Científica, v. 17, no. 2, p. 169-192, doi: 10.11606/issn.2316-9095.v17-455

Nomade, S., K. B. Knight, E. Beutel, P. R. Renne, C. Verati, G. Féraud, A. Marzoli, N. Youbi, and H. Bertrand, 2007, Chronology of the Central Atlantic Magmatic Province:

implications for the Central Atlantic rifting processes and the Triassic–Jurassic biotic crisis: Palaeogeography Palaeoclimatology Palaeoecology v. 244, p. 326-344, doi: 10.1016/j.palaeo.2006.06.034

Oliveira, A. L., M. M. Pimentel, R. A. Fuck, and D. C. Oliveira, 2018, Petrology of Jurassic and Cretaceous basaltic formations from the Parnaíba Basin, NE Brazil: correlations and associations with large igneous provinces. Geological Society, London, Special Publications, v. 472, p. SP472-5. https://doi.org/10.1144/SP472.5

Oliveira, D. C., and W.U. Mohriak, 2003, Jaibaras trough: an important element in the early tectonic evolution of the Parnaíba interior sag basin, Northern Brazil: Marine and Petroleum geology, v. 20, no. 3-4, p. 351-383, doi: 10.1016/S0264-8172(03)00044-8

Poelchau, H. S., D. R. Baker, T. Hantschel, B. Horsfield, and B. Wygrala, 1997, Basin simulation and the design of the conceptual basin model, *in* D. H. Welte, B. Horsfield, and D. R. Baker, eds., Petroleum and basin evolution: insights from petroleum geochemistry, geology and basin modeling: Springer Science & Business Media, p. 3-70, doi: 10.1007/978-3-642-60423-2_2

Porto, A. L., and E. Pereira, 2014, Seismic Interpretation of Igneous Intrusions and Their Implications for an Unconventional Petroleum System in Southeastern Parnaíba Basin, Northeastern Brazil: AGU Fall Meeting, San Francisco, USA, December 15-19, 2014, doi: 2014AGUFM.V51B4753P

Rahn, M. K., M. T. Brandon, G. E. Batt, and J. I. Garver, 2004, A zero-damage model for fission-track annealing in zircon: American Mineralogist, v. 89, no. 4, p. 473-484, doi: 10.2138/am-2004-0401

Rickard, D., 1997, Kinetics of pyrite formation by the H2S oxidation of iron (II) monosulfide in aqueous solutions between 25 and 125 C: the rate equation: Geochimica et Cosmochimica Acta, v. 61, no. 1, p. 115-134, doi: 10.1016/S0016-7037(96)00321-3

Rodrigues, R., 1995, A Geoquímica Orgânica na Bacia do Parnaíba, Doctoral's thesis, Instituto de Geociências/Universidade Federal do Rio Grande do Sul, Porto Alegre, RS, 252 p.

Senger, K., J. Millett, S. Planke, K. Ogata, C. H. Eide, M. Festøy, O. Galland, and D. A. Jerram, 2017, Effects of igneous intrusions on the petroleum system: a review: First Break, v. 35, no. 6, p. 47-56, doi: 10.3997/1365-2397.2017011

Silva, A. G. D., C. N. D. Almeida, S. D. C. Valente, and L. F. B. D. Almeida, 2017, The petrogenesis of tholeiitic diabases in eastern Parnaíba Basin: evidence for geochemical heterogeneities in the subcontinental lithospheric mantle in NE Brazil: Brazilian Journal of Geology, v. 47, no. 1, p. 109-126, doi: 10.1590/2317-4889201720160041

Svensen, H. H., T. H. Torsvik, S. Callegaro, L. Augland, T. H. Heimdal, D. A. Jerram, S. Planke, and E. Pereira, 2018, Gondwana Large Igneous Provinces: plate reconstructions, volcanic basins and sill volumes: Geological Society, London, Special Publications, v. 463, no. 1, p. 17-40, doi: https://doi.org/10.1144/SP463.7

Taylor, K. G., and J. H. S. Macquaker, 2000, Early diagenetic pyrite morphology in a mudstone-dominated succession: The Lower Jurassic Cleveland Ironstone Formation, eastern England: Sedimentary Geology, v. 131, no. 1-2, p. 77-86, doi: 10.1016/S0037-0738(00)00002-6

Taylor, T. R., M. R. Giles, L. A. Hathon, T. N. Diggs, N. R. Braunsdorf, G. V. Birbiglia, M. G. Kittridge, C. I. Macaulay, and I. S. Espejo, 2010, Sandstone diagenesis and reservoir quality prediction: Models, myths, and reality: AAPG bulletin, v. 94, no. 8, p. 1093-1132, doi: 10.1306/04211009123

Thomaz Filho, A., A. M. P. Mizusaki, E. J. Milani, and P. de Cesero, 2000, Rifting and magmatism associated with the South America and Africa break up: Brazilian Journal of Geology, v. 30, no. 1, p. 017-019.

Thomaz Filho, A., A. M. P. Mizusaki, and L. Antonioli, 2008, Magmatism and petroleum exploration in the Brazilian Paleozoic basins: Marine and petroleum geology, v. 25, no. 2, p. 143-151, doi: 10.1016/j.marpetgeo.2007.07.006

Vandenbroucke, M., F. Behar, and J. L. Rudkiewicz, 1999, Kinetic modeling of petroleum formation and cracking: implications from the high pressure/high temperature Elgin Field (UK, North Sea): Organic Geochemistry, v. 30, no. 9, p. 1105-1125, doi: 10.1016/S0146-6380(99)00089-3

Vaz, P. T., N. G. A. M. Rezende, J. R. Wanderley Filho, and W. S. Travassos, 2007, Bacia do Parnaíba: Boletim de Geociências da PETROBRAS, v. 15, no. 2, p. 253-263.

Verdel, C., B. A. van der Pluijm, and N. Niemi, 2012, Variation of illite/muscovite 40 Ar/39 Ar age spectra during progressive low-grade metamorphism: an example from the US Cordillera: Contributions to Mineralogy and Petrology, v. 164, no. 3, p. 521-536, doi: 10.1007/s00410-012-0751-7

Vermeesch, P., 2009, RadialPlotter: A Java application for fission track, luminescence and other radial plots: Radiation Measurements, v. 44, no. 4, p. 409-410, doi: 10.1016/j.radmeas.2009.05.003

Vieira, L.V., and C. M. S. Scherer, 2017, Facies architecture and high resolution sequence stratigraphy of an aeolian, fluvial and shallow marine system in the Pennsylvanian Piauí Formation, Parnaíba Basin, Brazil: Journal of South American Earth Sciences, v. 76, p. 238-256, doi: https://doi.org/10.1016/j.jsames.2017.03.009

Welte, D. H., B. Horsfield, and D. R. Baker, 2012, Petroleum and basin evolution: insights from petroleum geochemistry, geology and basin modeling: Berlin, Springer Science & Business Media, 535 p.

Wilkinson, M., K. L. Milliken, and R. S. Haszeldine, 2001, Systematic destruction of K-feldspar in deeply buried rift and passive margin sandstones: Journal of the Geological Society, v. 158, no. 4, p. 675-683, doi:10.1144/jgs.158.4.675

Worden, R. H., and S. Morad, 2003, Clay minerals in sandstones: controls on formation, distribution and evolution, *in* R. H. Worden and S. Morad, eds., Clay Mineral Cements in Sandstones: Blackwell Publishing Ltd, p. 1-41, doi:10.1002/9781444304336.ch1

Yalçin, M. N., R. Littke, and R. F. Sachsenhofer, 1997, Thermal History of Sedimentary Basins, *in* D. H. Welte, B. Horsfield, and D. R. Baker, eds., Petroleum and basin evolution: insights from petroleum geochemistry, geology and basin modeling: Springer Science & Business Media, p. 71-167, doi: 10.1007/978-3-642-60423-2_3

Zalán, P. V., 2004, Evolução fanerozóica das bacias sedimentares brasileiras, *in* V. Mantesso-Neto, A. Bartorelli, C. D. R. Carneiro, and B. B. Brito-Neves, eds., Geologia do continente sul-americano: evolução da obra de Fernando Flávio Marques de Almeida: São Paulo, Beca, p. 595-613.

REFERÊNCIAS

ALMEIDA, F. F. M.; CARNEIRO, C. D. R. Inundações marinhas fanerozóicas no Brasil e recursos minerais associados. In: MANTESSO-NETO, V.; BARTORELLI, A.; CARNEIRO, C. D. R.; BRITO-NEVES, B. B. (Org.). *Geologia do continente sul-americano: evolução da obra de Fernando Flávio Marques de Almeida*. São Paulo: Beca, 2004. p. 43-58.

ANP. *Bacia do Parnaíba: Sumário Geológico e Setores em Oferta – 13ª Rodada de Licitações,* 2015. Disponível em:<http://www.anp.gov.br/>. Acesso em outubro, 2017.

ARAÚJO, R. N.; NOGUEIRA, A. C. R.; BANDEIRA, J.; ANGÉLICA, R. S. Shallow lacustrine system of the Permian Pedra de Fogo Formation, Western Gondwana, Parnaíba Basin, Brazil. *Journal of South American Earth Sciences*, v. 67, p. 57-70, 2016.

ARMSTRONG, P. A. Thermochronometers in sedimentary basins. *Reviews in Mineralogy and Geochemistry*, v. 58, n. 1, p. 499-525, 2005.

BAKSI, A. K.; ARCHIBALD, D. A. Mesozoic igneous activity in the Maranhão province, northern Brazil: 40Ar/39Ar evidence for separate episodes of basaltic magmatism. *Earth and Planetary Science Letters*, v. 151, n. 3-4, p. 139-153, 1997.

BERNET, M.; GARVER, J. I. Fission-track analysis of detrital zircon. *Reviews in Mineralogy and Geochemistry*, v. 58, n. 1, p. 205-237, 2005.

CARDOSO, A. R.; NOGUEIRA, A. C. R.; ABRANTES, F. R.; RABELO, C. E. N. Mesozoic lacustrine system in the Parnaíba Basin, northeastern Brazil: Paleogeographic implications for west Gondwana. *Journal of South American Earth Sciences*, v. 74, p. 41-53, 2017.

CPRM. *Serviço Geológico Do Brasil (CPRM) - Geobank.* 2005. Disponível em:<http://geobank.cprm.gov.br/>. Acesso em outubro, 2017.

DODSON, M. H. Closure temperature in cooling geochronological and petrological systems. *Contributions to Mineralogy and Petrology*, v. 40, n. 3, p. 259-274, 1973.

DONELICK, R. A. Method of fission track analysis utilizing bulk chemical etching of apatite. *U.S. Patent* v. 5, p. 267-274, 1993.

DONELICK, R. A.; O'SULLIVAN, P. B.; KETCHAM, R. A. Apatite fission-track analysis. *Reviews in Mineralogy and Geochemistry*, v. 58, n. 1, p. 49-94, 2005.

FODOR, R. V.; SIAL, A. N.; MUKASA, S. B.; MCKEE, E. H. Petrology, isotope characteristics, and K-Ar ages of the Maranhao, northern Brazil, Mesozoic basalt province. *Contributions to Mineralogy and Petrology*, v. 104, n. 5, p. 555-567, 1990.

GALBRAITH, R. F.; LASLETT, G. M. Statistical models for mixed fission track ages. *Nuclear tracks and radiation measurements*, v. 21, n. 4, p. 459-470, 1993.

GARVER, J. I.; REINERS, P. W.; WALKER, L. J.; RAMAGE, J. M.; PERRY, S. E. Implications for Timing of Andean Uplift from Thermal Resetting of Radiation-Damaged Zircon in the Cordillera Huayhuash, Northern Peru. *The Journal of Geology,* v. 113, p. 117-138. 2005.

GALLAGHER, K.; BROWN, R.; JOHNSON, C. Fission track analysis and its applications to geological problems. *Annual Review of Earth and Planetary Sciences*, v. 26, n. 1, p. 519-572, 1998.

GÓES, A. M. *Formação Poti (Carbonífero inferior) da Bacia do Parnaíba*. 1995. Tese (Doutorado em Geologia) – Instituto de Geociências, Universidade de São Paulo, São Paulo.

GÓES, A. D. O.; FEIJÓ, F. J. Bacia do Parnaíba. *Boletim de Geociências da PETROBRÁS*, v. 8, n. 1, p. 57-67, 1994.

HURFORD, A. J.; GREEN, P. F. The zeta age calibration of fission-track dating. *Chemical Geology*, v. 41, p. 285-317, 1983.

KETCHAM, R. A.; DONELICK, R. A.; CARLSON, W. D. Variability of apatite fission-track annealing kinetics: III. Extrapolation to geological time scales. *American Mineralogist*, v. 84, n. 9, p. 1235-1255, 1999.

LASLETT, G. M.; GREEN, P. F.; DUDDY, I. R.; GLEADOW, A. J. W. Thermal annealing of fission tracks in apatite 2. A quantitative analysis. *Chemical Geology: Isotope Geoscience Section*, v. 65, n. 1, p. 1-13, 1987.

LISKER, F.; VENTURA, B.; GLASMACHER, U. A. Apatite thermochronology in modern geology. *Geological Society, London, Special Publications*, v. 324, n. 1, p. 1-23, 2009.

MARZOLI, A.; RENNE, P. R., PICCIRILLO, E. M.; ERNESTO, M., BELLIENI, G.; DE MIN, A. Extensive 200-million-year-old continental flood basalts of the Central Atlantic Magmatic Province. *Science*, v. 284, n. 5414, p .616-618. 1999.

MERLE, R.; MARZOLI, A.; BERTRAND, H.; REISBERG, L.; VERATI, C.; ZIMMERMANN, C.; CHIARADIA, M.; BELLIENI, G.; ERNESTO, M. 40 Ar/39 Ar ages and Sr–Nd–Pb–Os geochemistry of CAMP tholeiites from Western Maranhão basin (NE Brazil). *Lithos*, v. 122, n. 3, p. 137-151, 2011.

MILANI, E. J.; ZALÁN, P. V. An outline of the geology and petroleum systems of the Paleozoic interior basins of South America. *Episodes*, v. 22, p. 199-205, 1999.

MORA, A.; HORTON, B. K.; MESA, A.; RUBIANO, J.; KETCHAM, R. A.; PARRA, M.; BLANCO, V.; GARCIA, D.; STOCKLI, D. F. Migration of Cenozoic deformation in the Eastern Cordillera of Colombia interpreted from fission track results and structural relationships: Implications for petroleum systems. *AAPG bulletin*, v. 94, n. 10, p. 1543-1580, 2010.

OLIVEIRA, D. C.; MOHRIAK, W. U. Jaibaras trough: an important element in the early tectonic evolution of the Parnaíba interior sag basin, Northern Brazil. *Marine and Petroleum geology*, v. 20, n. 3-4, p. 351-383, 2003.

OSADETZ, K. G.; KOHN, B. P.; FEINSTEIN, S.; O'SULLIVAN, P. B. Thermal history of Canadian Williston basin from apatite fission-track thermochronology—implications for petroleum systems and geodynamic history. *Tectonophysics*, v. 349, n. 1-4, p. 221-249, 2002.

REINERS, P. W.; BRANDON, M. T. Using thermochronology to understand orogenic erosion. *Annual Review of Earth Planetary Sciences*, v. 34, p. 419-466, 2006.

RODRIGUES, R. A Geoquímica Orgânica na Bacia do Parnaíba. 1995. Tese (Doutorado em Geologia) – Instituto de Geociências, Universidade Federal do Rio Grande do Sul, Porto Alegre.

ROSSETTI, D. F.; GÓES, A. M.; ARAI, M. A passagem aptiano-albiano na Bacia do Grajaú, MA. In: ROSSETTI, D. F.; GÓES, A. M.; TRUCKENBRODT, W. (Org.). *O Cretáceo na Bacia de São Luís-Grajaú*. Belém: Museu Paraense Emilio Goeldi, 2001. p. 101-117.

SILVA, A. G. D.; ALMEIDA, C. N. D.; VALENTE, S. D. C.; ALMEIDA, L. F. B. D. The petrogenesis of tholeiitic diabases in eastern Parnaíba Basin: evidence for geochemical heterogeneities in the subcontinental lithospheric mantle in NE Brazil. *Brazilian Journal of Geology*, v. 47, n. 1, p. 109-126, 2017.

TAGAMI, T. Zircon fission-track thermochronology and applications to fault studies. *Reviews in Mineralogy and Geochemistry*, v. 58, n. 1, p. 95-122, 2005.

TAGAMI, T.; O'SULLIVAN, P. B. Fundamentals of fission-track thermochronology. *Reviews in Mineralogy and Geochemistry*, v. 58, n. 1, p. 19-47, 2005.

TINGATE, P. R.; DUDDY, I. R. The thermal history of the eastern Officer Basin (South Australia): evidence from apatite fission track analysis and organic maturity data. *Tectonophysics*, v. 349, n. 1-4, p. 251-275, 2002.

WAGNER G. A. Correction and Interpretation of Fission Track Ages. In: JÄGER E., HUNZIKER J. C. (Org.) *Lectures in Isotope Geology*. Berlin: Springer, 1979. p. 170-177.

VAZ, P. T.; REZENDE, N. G. A. M.; WANDERLEY FILHO, J. R.; TRAVASSOS, W. A. S. Bacia do Parnaíba. *Boletim de Geociências da PETROBRÁS*, v. 15, n. 2, p. 253-263, 2007.

VIEIRA, L. V.; SCHERER, C. M. Facies architecture and high resolution sequence stratigraphy of an aeolian, fluvial and shallow marine system in the Pennsylvanian Piauí Formation, Parnaíba Basin, Brazil. *Journal of South American Earth Sciences*, v. 76, p. 238-256. 2017.

CONFIRMAÇÃO DE SUBMISSÃO DO ARTIGO

Submission Confirmation for AAPG Bulletin BLTN18-117

E

em.bltn.0.5b425f.0f914911@editorialmanager.com em nome de AAPG Bulletin <em@editorialman

Responder a todos |

Ontem, 17:58

Marcio Cardoso Junior

RE: BLTN18-117

Dear Mr. Cardoso Jr.,

Your submission entitled "THERMAL HISTORY OF POTENTIAL GAS RESERVOIR ROCKS IN THE EASTERN PARNAÍBA BASIN, BRAZIL" has been received by journal AAPG Bulletin

You will be able to check on the progress of your paper by logging on to Editorial Manager as an author. The URL is https://bltn.editorialmanager.com/.

Your manuscript will be given a reference number once an Editor has been assigned.

Thank you for submitting your work to this journal.

Kind regards,

AAPG Bulletin